Tectonics

RESEARCH ARTICLE
10.1029/2020TC006415

Key Points:

- Thermal modeling reveals a stepwise history composed of two rapid cooling phases for Albian to Campanian and Eocene times
- The first phase relates with the exhumation of the Paleozoic basement promoted by the uplift and erosion of a broad N-S striking antiform
- The second phase involves the inversion of the Manchana Covunco fault and the deformation of the Mesozoic sedimentary cover

Supporting Information:

Supporting Information may be found in the online version of this article.

Correspondence to:

A. Galetto,
antogaletto@gmail.com

Citation:

Galetto, A., Georgieva, V., García, V. H., Zattin, M., Sobel, E. R., Glodny, J., et al. (2021). Cretaceous and Eocene rapid cooling phases in the Southern Andes (36°–37°S): Insights from low-temperature thermochronology, U-Pb geochronology, and inverse thermal modeling from Domuyo area, Argentina. *Tectonics*, *40*, e2020TC006415. https://doi.org/10.1029/2020TC006415

Received 10 JUL 2020
Accepted 7 MAY 2021

Cretaceous and Eocene Rapid Cooling Phases in the Southern Andes (36°–37°S): Insights From Low-Temperature Thermochronology, U-Pb Geochronology, and Inverse Thermal Modeling From Domuyo Area, Argentina

A. Galetto[1,2], V. Georgieva[3], V. H. García[1,4], M. Zattin[5], E. R. Sobel[4], J. Glodny[6], S. Bordese[7], G. Arzadún[1,7], F. Bechis[1,8], A. T. Caselli[1,9], and R. Becchio[1,10]

[1]Consejo Nacional de Investigaciones Científicas y Técnicas (CONICET), Buenos Aires, Argentina, [2]Universidad de Buenos Aires, Ciudad Universitaria, Buenos Aires, Argentina, [3]Universidad Austral de Chile, Instituto de Ciencias de la Tierra/Instituto de Ciencias Físicas y Matemáticas, Valdivia, Chile, [4]Institut für Geowissenschaften, Universität Potsdam, Potsdam-Golm, Germany, [5]Department of Geosciences, University of Padova, Padova, Italy, [6]GFZ German Research Centre for Geosciences, Potsdam, Germany, [7]Laboratorio de Termocronología La.Te. Andes S.A., Vaqueros, Argentina, [8]Universidad Nacional de Río Negro, San Carlos de Bariloche, Río Negro, Argentina, [9]Universidad Nacional de Río Negro, General Roca, Río Negro, Argentina, [10]Universidad Nacional de Salta, Salta, Argentina

Abstract The integration of inverse thermal history modeling of new geochronological data with structural analyses from the western flank of the Domuyo volcano (~36°30′S) allows us to propose a detailed cooling history of a key region in the Southern Andes. The Domuyo area is located in the northwestern part of the Chos Malal fold-and-thrust belt in the back-arc of the Southern Andes. Despite extensive geological investigations in this region, details about the early stages of Andean deformation remain poorly understood. The present study focuses on the interpretation and integration of new U-Pb, fission track, and (U-Th-Sm)/He data constraining the Cretaceous to Paleogene exhumation history of the Southern Andes at these latitudes. The results indicate two main episodes of rapid cooling during Albian-Campanian and Eocene times that can be related to exhumation driven by two main contractional pulses. The first event promoted basement cooling/exhumation associated with the uplift and erosion of a broad N-S striking antiform; whereas the Eocene episode triggered the inversion of the preexisting N-S striking Manchana Covunco normal fault and the deformation of the Mesozoic sedimentary cover. The two orogenic phases are separated by a potential period of orogenic quiescence during the Paleocene. These new insights highlight the importance of the initial compressional stages of mountain building in the Southern Andes at these latitudes.

1. Introduction

The westward acceleration of the South American plate after the opening of the Southern Atlantic Ocean during the Late Cretaceous has been regarded as the driving mechanism for the onset of contractional tectonics along the western margin of South America, ultimately promoting the inversion of Mesozoic back-arc basins and the formation of the Andean mountain chain (Ramos, 2009; Somoza & Zaffarana, 2008) (Figure 1). Since then, deformation processes have been mainly controlled by the geometry of the oceanic slab and the rate and obliquity of convergence between the subducting and South American plates (e.g., Mpodozis & Ramos, 1990; Ramos, 2009; Somoza & Ghidella, 2005), the collision of oceanic ridges (e.g., Fennell et al., 2019; Maloney et al., 2013; Seton et al., 2012), and the variability of the oceanic plate buoyancy promoting flattening and/or steepening of the subducting slab (Molnar & Atwater, 1978; Horton, 2018; Ramos & Folguera, 2009; Ramos & Kay, 2006).

Over the last two decades, numerous sedimentological, stratigraphic, structural, and geochronological studies have addressed different orogenic phases in the Southern Andes between 36°S and 39°S since Cretaceous times (Figures 2 and 3, and references therein). Thermochronological dating tools, including fission track and (U-Th-Sm)/He dating in apatites and zircons, have become established techniques to reconstruct the exhumation history of this region. The Chos Malal fold-and-thrust belt (ChMFTB) is located in the back-arc

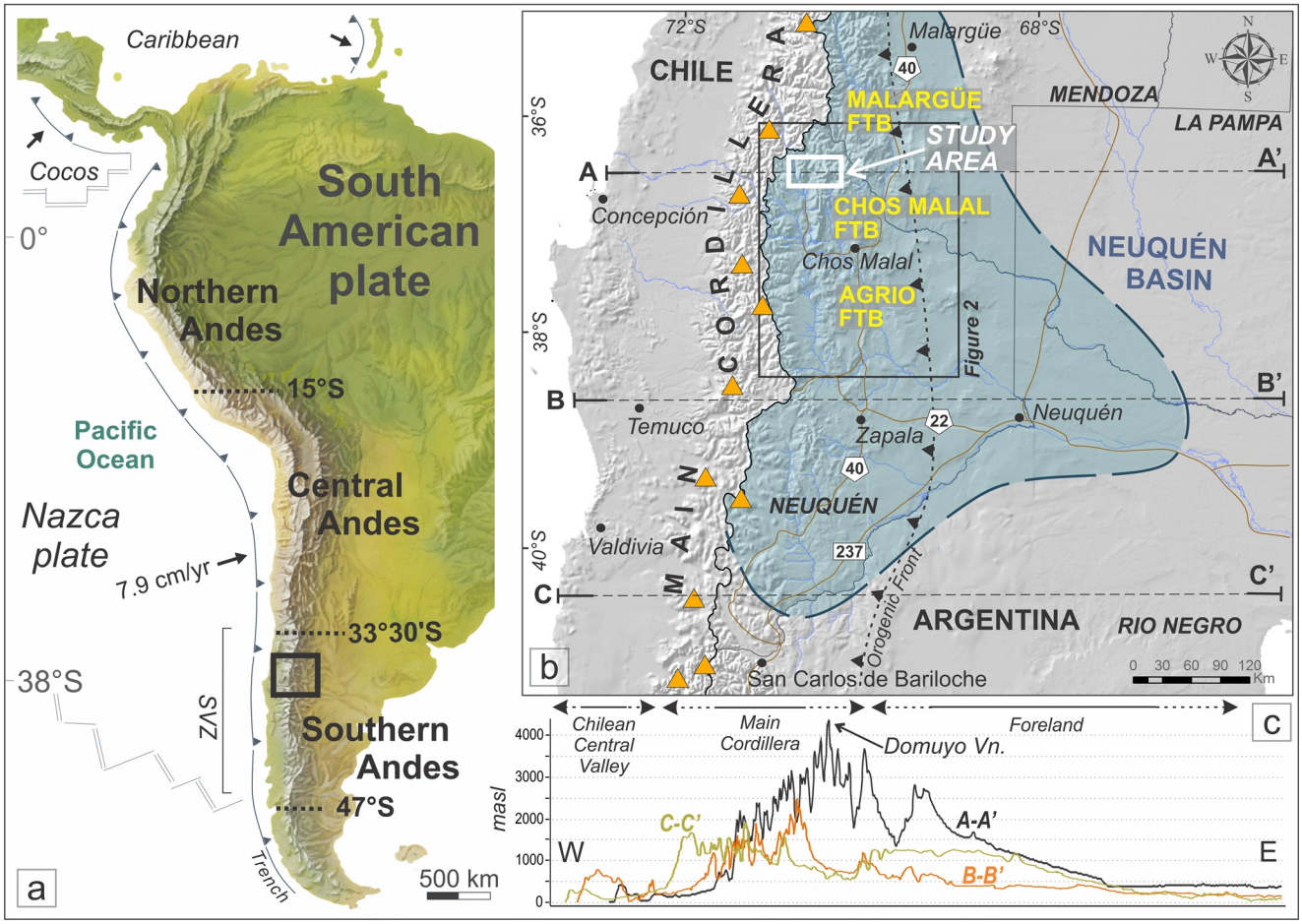

Figure 1. (a) Regional digital elevation model (DEM) showing the location of the study area (black box) in the Southern Andes (Tassara & Yáñez, 2003) at ~36°30′S and the Southern Volcanic Zone (SVZ) between 33°30′ and 47°S (Stern, 2004). (b) Shaded relief map showing the study area in the context of the Neuquén Basin and the main fold-and-thrust belts (FTB). (c) E-W elevation profiles across the study area at ~36°30′S (A-A′) and further south (B-B′ and C-C′).

of the Southern Andes between ~36°30′S and 37°30′S (Figures 1 and 2). The relative magnitude and timing of the different tectonic phases responsible for its genesis are still a matter of debate. While the beginning of mountain building at these latitudes is suggested as latest Early to Late Cretaceous times (Di Giulio et al., 2012, 2016; Fennell et al., 2015; Gómez et al., 2019; Tunik et al., 2010), the oldest low-temperature thermochronological data indicate that the exhumation in the ChMFTB did not take place before ~72 Ma (Rojas Vera et al., 2015; Sánchez et al., 2018, 2020; Zamora Valcarce et al., 2009). Structural analysis and inverse thermal history modeling of apatite fission track data reveal a Late Cretaceous-Paleogene cooling episode, interpreted as the main compressive phase of the ChMFTB (Rojas Vera et al., 2015). In turn, thermochronological and detailed structural studies suggest that deeper levels of exhumation in the ChMFTB occurred during the middle-late Miocene (Folguera et al., 2007; Sánchez et al., 2018). Another field for open questions relates to the role of Paleogene deformation in this region. In the Frontal/Principal Cordillera fold-and-thrust belt (30°S), thermochronological analysis reveals that rapid Eocene exhumation is responsible for a significant buildup of topography and relief (Lossada et al., 2017), whereas in the ChMFTB, the Paleogene deformation episode is described as negligible (Sagripanti et al., 2012). Some local structural and geophysical studies suggest a certain impact of the Paleogene orogenic phase at 36°–37°S (Cobbold & Rossello, 2003), but no thermochronological studies support the existence of a rapid exhumation/cooling strictly linked to this phase at these latitudes.

We present new thermochronological data (fission track and (U-Th-Sm)/He in apatites and zircons) from Permian intrusives and Upper Jurassic sedimentary rocks, used for thermal history modeling in order to better constrain an updated tectonic evolution model for the western flank of the Domuyo area (~36°30′S;

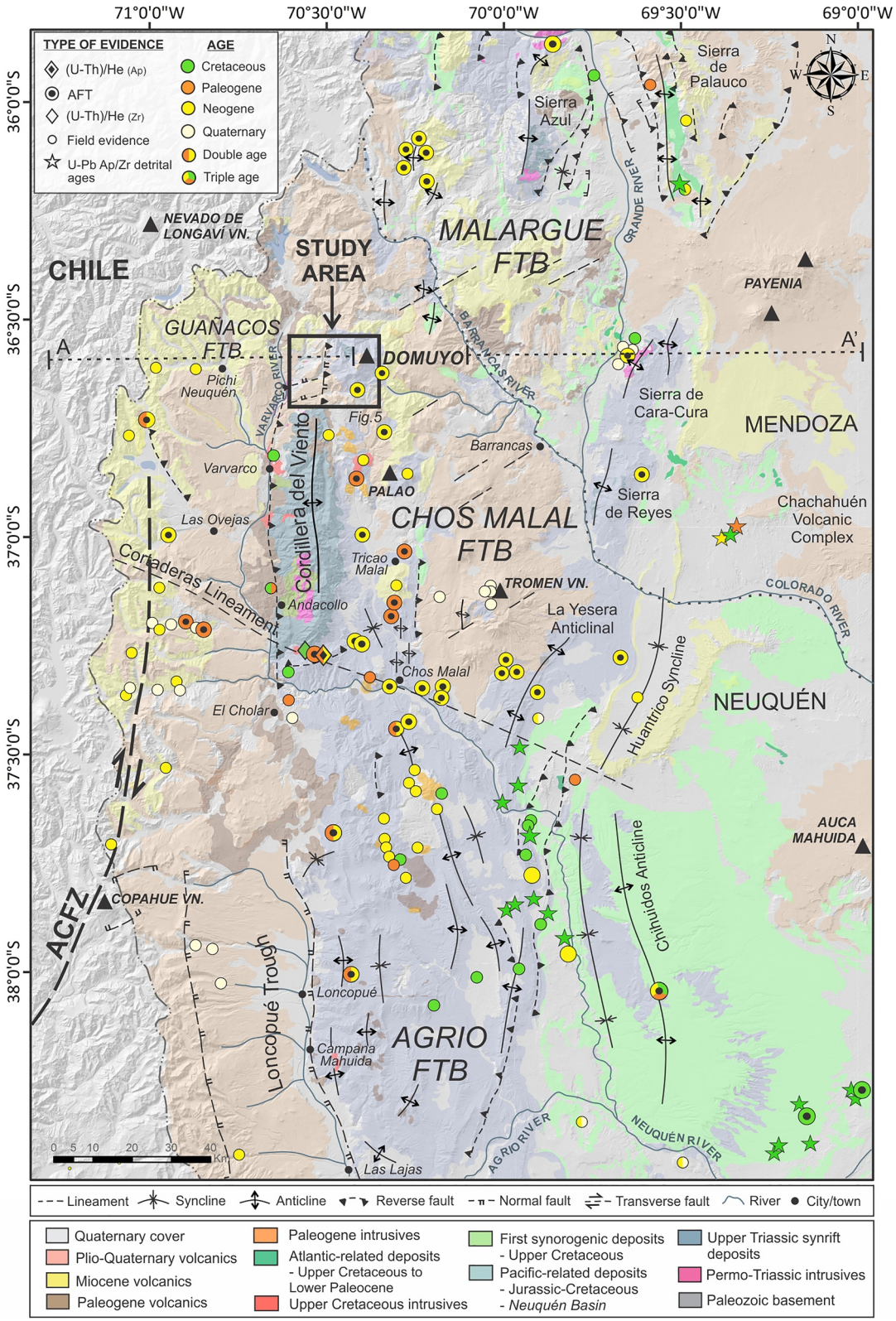

Figure 2. Evidence of compressive deformation documented in the Southern Andes of Argentina between 35°45′S and 38°30′S, together with the main lithological groups. The map shows a compilation of cooling ages which the authors infer to be related to deformation (Burns, 2002; Burns et al., 2006; Di Giulio et al., 2016; Folguera et al., 2015; Jordan et al., 2001; Muñoz, 1996; Rojas Vera et al., 2015; Sánchez et al., 2018, 2020; Thomson et al., 2010; Zamora Valcarce et al., 2009). FTB, fold-and-thrust belt; ACFZ, Antiñir-Copahue Fault Zone.

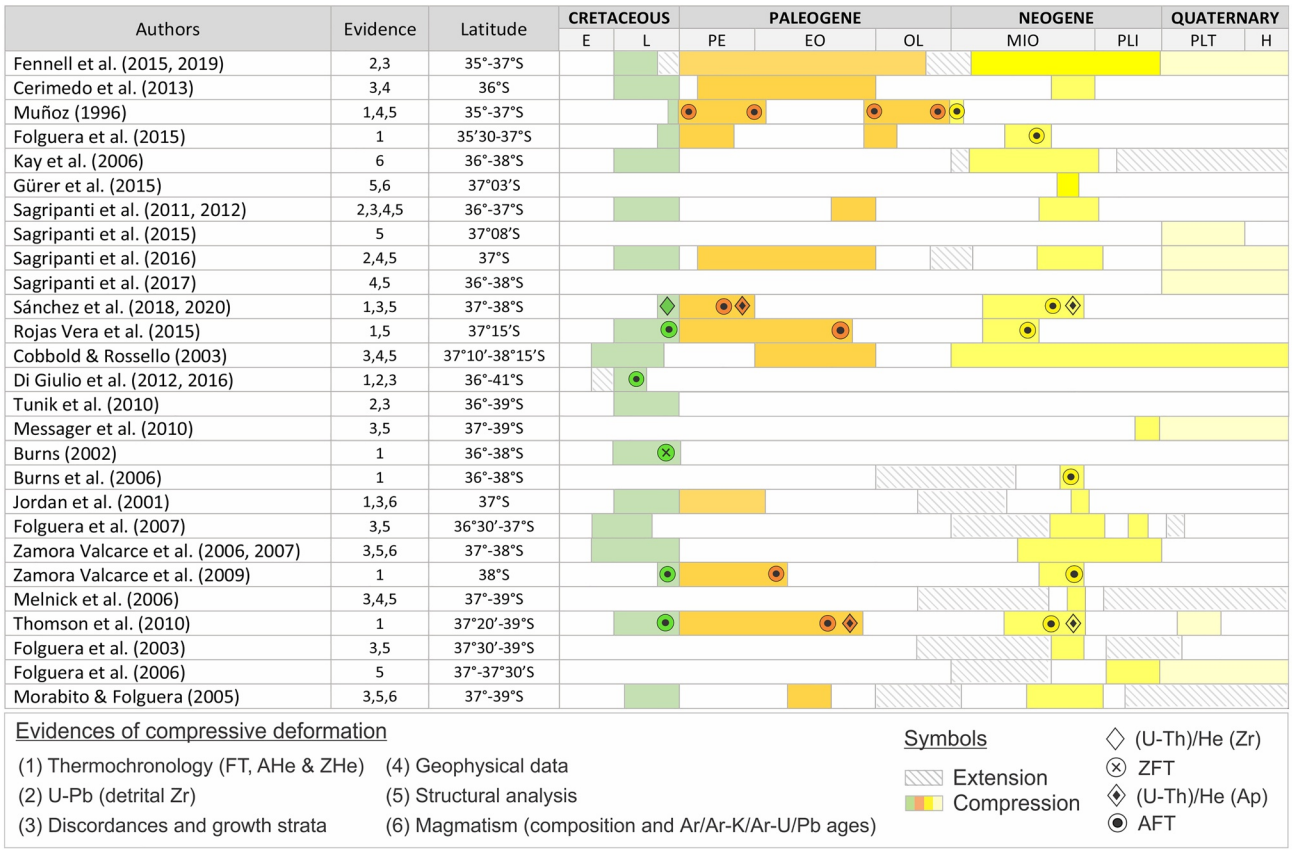

Figure 3. Summary of the evidence for compressive deformational episodes documented in the back-arc of the Southern Andes compiled in Figure 2. The compressive periods inferred from low-temperature thermochronometers by each author are highlighted with circles and rhombuses. The colors used for each deformational age and thermochronological evidence (circles and rhombuses) are equivalent to those used in Figure 2. Interpreted extensional periods are also indicated.

Figures 1 and 2). The application of multiple thermochronometers allows for the reconstruction of thermal histories across a wide spectrum of temperatures, reducing uncertainties, and leading to an improved analysis of the exhumation process (e.g., Hurford, 1986; Moore & England, 2001). Moreover, as the absolute age of Permian intrusives from Domuyo area was still under debate due to some similarities with Upper Cretaceous intrusives outcropping in the western foothills of Cordillera del Viento, we combined their thermochronological data with new U-Pb dating. These results allowed us to constrain the crystallization age of these intrusives and to model them using improved chronological data. Consequently, the results obtained in this study integrated with our structural data from the area (Galetto et al., 2018) represent a robust contribution toward understanding the exhumation and tectonic evolution of the Domuyo area in the framework of the Chos Malal fold-and-thrust belt, and to reevaluate the significance of the first compressive periods at these latitudes.

2. Geological Setting

The oldest rocks in the Domuyo area are represented by Upper Devonian meta-greywackes affected by contractional deformation to form tight subvertical to vertical folds, with a slight W-WSW vergence, related to the final stages of the Famatinian orogeny (Giacosa et al., 2014; Zappettini et al., 1987, 2012). Late Paleozoic mountain building processes (San Rafael orogeny) led to the formation of a continental-scale NW-SE trending mountain belt (Gondwanides). The gravitational collapse of this orogen during early Permian to Middle Triassic times was accompanied by widespread magmatic activity represented by granitoids and volcanic rocks that integrate the Choiyoi Group (Llambías & Sato, 2011) (Figure 4). Synchronous exhumation processes formed the Huarpic erosional surface on top of the Choiyoi Group intrusives marking the end of

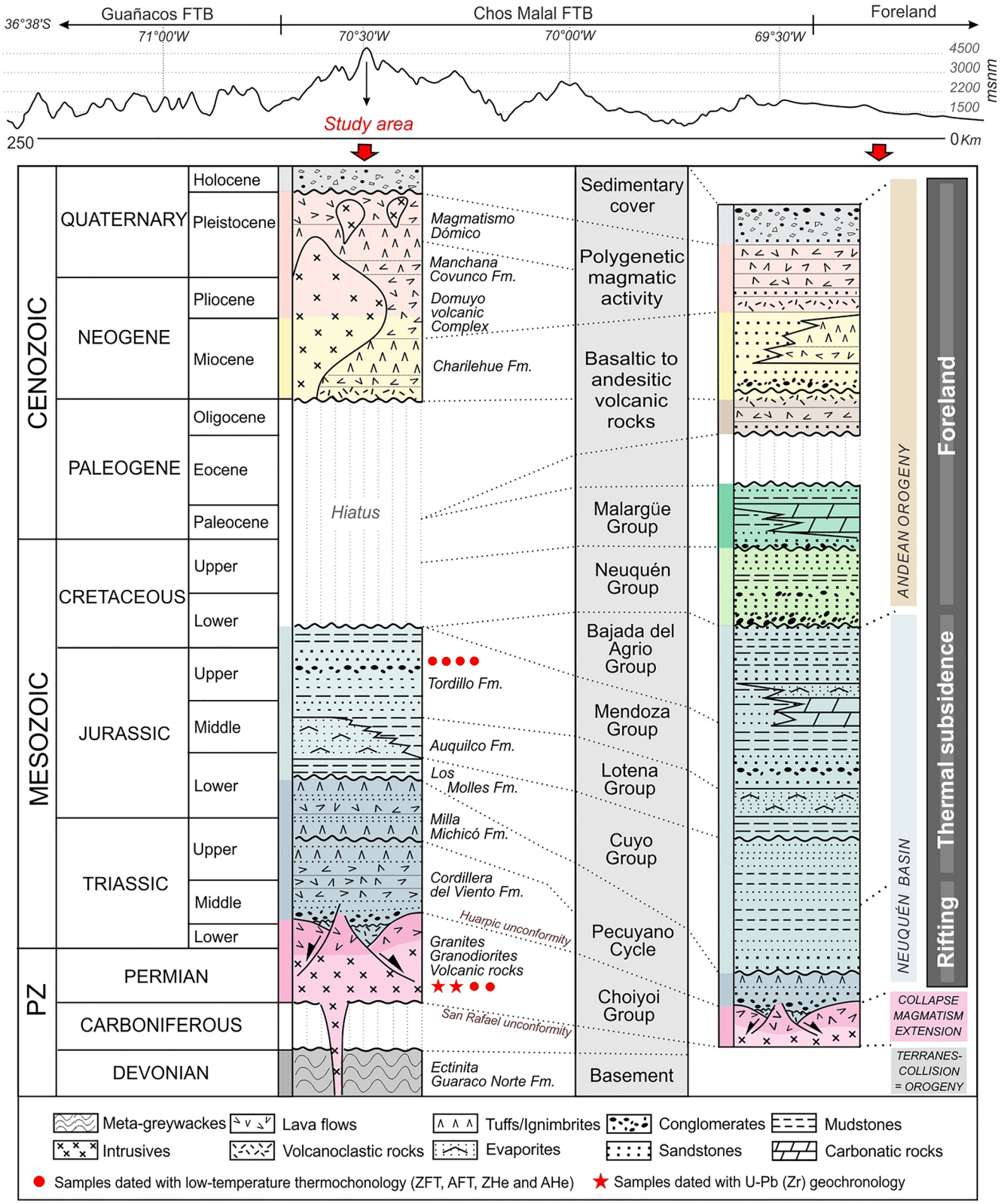

Figure 4. Simplified stratigraphic chart of the study area and its comparison to the foreland sequence (based on Arregui et al., 2011; JICA, 1983, 1984; Llambías et al., 1978, 2007; Miranda et al., 2006; Nullo et al., 2005; Orts et al., 2012; Sagripanti et al., 2011, 2012). Colors of lithological groups correspond to those used in Figure 2.

the Gondwanic Cycle (Azcuy & Caminos, 1987; Llambías et al., 2007). The Upper Devonian metamorphic rocks together with the Choiyoi Group constitute the structural basement of the study area.

From Late Triassic to Early Jurassic times, extensional faulting associated with continental-scale rifting processes controlled the fragmentation of the Huarpic erosion surface and the development of rift zones throughout the western margin of Gondwana (Franzese & Spalletti, 2001; Müller et al., 2016; Vergani et al., 1995). In the study region, these processes gave rise to the development of the Neuquén Basin, a large marine embayment that accumulated up to 7,000 m of volcanoclastic, marine, and continental deposits prior to the Andean orogeny (Carbone et al., 2011) (Figures 1 and 4). The localized NNW-SSE to NW-SE trending normal faulting that characterized the early-rift stage of the Neuquén Basin changed to a transitional phase in Early to Middle Jurassic times, when fault-controlled subsidence was replaced by regional thermal subsidence, with a progressive waning of magmatic activity and the onset of the post-rift phase (Arregui et al., 2011; Franzese & Spalletti, 2001; Vergani et al., 1995). In the study area, the syn-rift phase is represented by volcanic and volcanoclastic deposits of the Precuyano Cycle, widely exposed along the Cordillera del Viento (Figures 2 and 4). The post-rift sag phases are represented by a succession of marine and continental deposits of the Cuyo (marine), Lotena (transitional), Mendoza (continental to deep marine), and Bajada del Agrio (transitional to continental) groups (Figures 2 and 4). Simultaneously to the deposition of Kimmeridgian continental deposits of the Mendoza Group, specifically sandstones and minor conglomerates of the Tordillo Formation, a second extensional setting is proposed for the northern Neuquén Basin in response to the initial opening of the Southern Atlantic Ocean and a trench roll-back along the subduction margin (Charrier, 2007; Charrier et al., 2007; Mescua et al., 2020; Vergara et al., 1995). At the same time, transpressive tectonics is recorded in southern Neuquén Basin along the proposed E-W suture of the North Patagonian cratonic block, controlling the uplift of the Huincul arch (Silvestro & Zubiri, 2008).

The beginning of the crustal shortening along the western South American plate by Late Mesozoic times promoted the deposition of the first continental synorogenic foreland deposits in the Neuquén Basin during the latest Early-Late Cretaceous, which integrate the Neuquén Group (Di Giulio, 2012; Fennell et al., 2015; Gómez et al., 2019; Tunik et al., 2010) (Figures 2 and 4). Conspicuously, thermochronological data from the Chos Malal fold-and-thrust belt (ChMFTB) suggest the onset of cooling and inferred exhumation at ~72 Ma, long after the initiation of synorogenic sedimentation (Rojas Vera et al., 2015; Sánchez et al., 2018, 2020; Zamora Valcarce et al., 2009) (Figures 2 and 3). The construction of the ChMFTB occurred through an interaction between first-order basement structures that characterize its inner part in the west and multiple decollement levels within the Mesozoic sedimentary rocks toward the foreland (Kozlowski et al., 1996; Sánchez et al., 2015; Turienzo et al., 2018). During Late Cretaceous to Paleocene times, intrusive and effusive magmatic activity occurred along the Andean axis (Casé et al., 2008; Franchini et al., 2003; Iannelli et al., 2020; Kay et al., 2006). The Paleocene magmatic activity recorded in the northern Neuquén province has been associated with diverse tectonic settings: (i) a potential postorogenic relaxation stage that followed the initial uplift of the Andes (Llambías & Aragón, 2011); (ii) a relative shallowing of the Benioff zone with the eastward migration of the arc front and major contractional deformation (Ramos & Kay, 2006; Spagnuolo et al., 2012); and recently, (iii) with an extensional tectonic episode in response to a southward migrating mid-oceanic ridge subduction between ~35°S and 37°S (Fennell et al., 2019; Iannelli et al., 2020). Synchronously with the magmatic activity, sedimentary rocks of the Malargüe Group were deposited on top of the Neuquén Basin deposits in the foreland area, representing the first Atlantic-related continental and marine succession (Aguirre-Urreta et al., 2010) (Figures 2 and 4).

Paleogene apatite fission track cooling ages of ~50–40 Ma from ChMFTB have been interpreted as the final stages of the Late Cretaceous orogenic phase (Rojas Vera et al., 2015; Sánchez et al., 2018, 2020; Zamora Valcarce et al., 2009). Conversely, geophysical and structural studies developed east of the Cordillera del Viento (~37°S) reveal Paleogene contractional deformation and crustal thickening in representation of a second independent compressive episode (Cobbold & Rossello, 2003). This compressive stage has been correlated with the Incaic orogenic phase widely recognized further north in the Cordillera Frontal and in the Puna/southern Altiplano where it represents the major stage of construction of the Andes (e.g., Hongn et al., 2007; Lossada et al., 2017; Steinmann, 1929). During the Paleogene, large parts of the ChMFTB and adjacent regions likely formed positive areas since some synorogenic deposits accumulated in a foreland basin north and south of the fold-and-thrust belt (Leanza & Hugo, 2001; Ramos & Kay, 2006).

Since the Oligocene to the early Miocene, regional extension invoked the development of the Cura Mallín basin in the intra-arc west of the study area, which was subsequently inverted by another major compressional stage during middle-late Miocene times; these episodes have been related to steepening and shallowing of the subducted oceanic slab, respectively (Folguera et al., 2007; Spikings et al., 2008; Utgé et al., 2009) (Figure 2). Cooling ages ranging from ~15 to ~7 Ma from the Agrio and Chos Malal fold-and-thrust belts have been associated with this last compressive pulse (Folguera et al., 2015; Sánchez et al., 2018, 2020). Toward the Plio-Pleistocene, the arc and retro-arc areas were subjected to renewed extension, promoting the development of Plio-Quaternary extensional basins and polygenic magmatic activity, including the Domuyo Volcanic Complex (Folguera et al., 2005; Galetto et al., 2018; Ramos & Kay, 2006; Rojas Vera et al. (2014a, 2014b) (Figures 2, 4 and 5). In turn, evidence of coeval Plio-Quaternary compressive deformation has been also reported for ~37°S (e.g., Colavitto et al., 2020; Galland et al., 2007; Messager et al., 2010).

3. Structural Framework of the Domuyo Area

The Domuyo volcano is considered one of the most voluminous Plio-Pleistocene igneous centers of the Southern Andes and it hosts one of the world's largest high-enthalpy geothermal fields, with an important present-day activity (Astort et al., 2019; Chiodini et al., 2014). Its underlying structure has been characterized as a broad basement antiform with a N-S axis gently plunging to the north, developed during the Andean orogeny and further deformed during the superimposed emplacement of the Domuyo Volcanic Complex (DVC) since middle Miocene-Pliocene times (Llambías et al., 1978). The DVC is composed by a granitic-dioritic porphyry stock interpreted as the upper section of a partly exposed middle Miocene-Pliocene magmatic chamber, complemented by volcanic rocks depicting a central magmatic system fed through preexisting fractures on the western flank of Domuyo volcano (Llambías et al., 1978; Miranda et al., 2006; Pesce, 1987, Figure 5).

The integration of detailed fracture analysis and kinematic studies of mesoscale faults with geological, structural, and geophysical data indicates that the structural architecture of the study area has been strongly controlled by the reactivation of basement structures (cf. Galetto et al., 2018). The main structure inferred along the western flank of the Domuyo volcano is the Manchana Covunco fault (MCF; Galetto et al., 2018). The MCF is a local N-S trending, east-dipping high-angle normal fault that likely controlled the thickness variations of the Mesozoic sedimentary rocks and has been partially inverted during the Andean orogeny. It is a blind structure buried by the Plio-Quaternary volcanic sequence and it exerts a first-order control on the present-day Domuyo geothermal field dynamics (Galetto et al., 2018). A set of ~E-W-striking basement faults intersects the MCF, related to the rifting phase of the Neuquén Basin, and coincident with the main geothermal manifestations (Figure 5). Kinematic analysis reveals a reactivation of preexisting basement faults likely associated with the accommodation of regional extension during Plio-Quaternary times (Galetto et al., 2018).

So far, both the onset of compressive deformation in the Domuyo area during the Andean orogeny and the subsequent development of its structural configuration preceding the emplacement of the DVC are poorly documented and therefore remain under debate. The main objective of this study is to shed light on these aspects by means of geochronological and thermochronological studies.

4. Methods

4.1. Sampling Methodology and Location of Samples

Six bedrock samples collected from the western flank of the Domuyo volcano were processed for apatite and zircon fission track, and (U-Th-Sm)/He analysis. For two of them, we also established U-Pb zircon data. Sampling localities were chosen to evaluate the history of the MCF by tracking exhumation-cooling episodes across the strike of the fault (e.g., Ehlers & Farley, 2003; Georgieva et al., 2016; Kelley, 2005; Strecker, 1996). Two samples from granites and granodiorites of the Choiyoi Group (TF12, TF16) and four samples from Upper Jurassic sandstones of the Tordillo Formation (TF09, TF10, TF17, TF18) were collected west and east of the MCF, respectively (Figure 5).

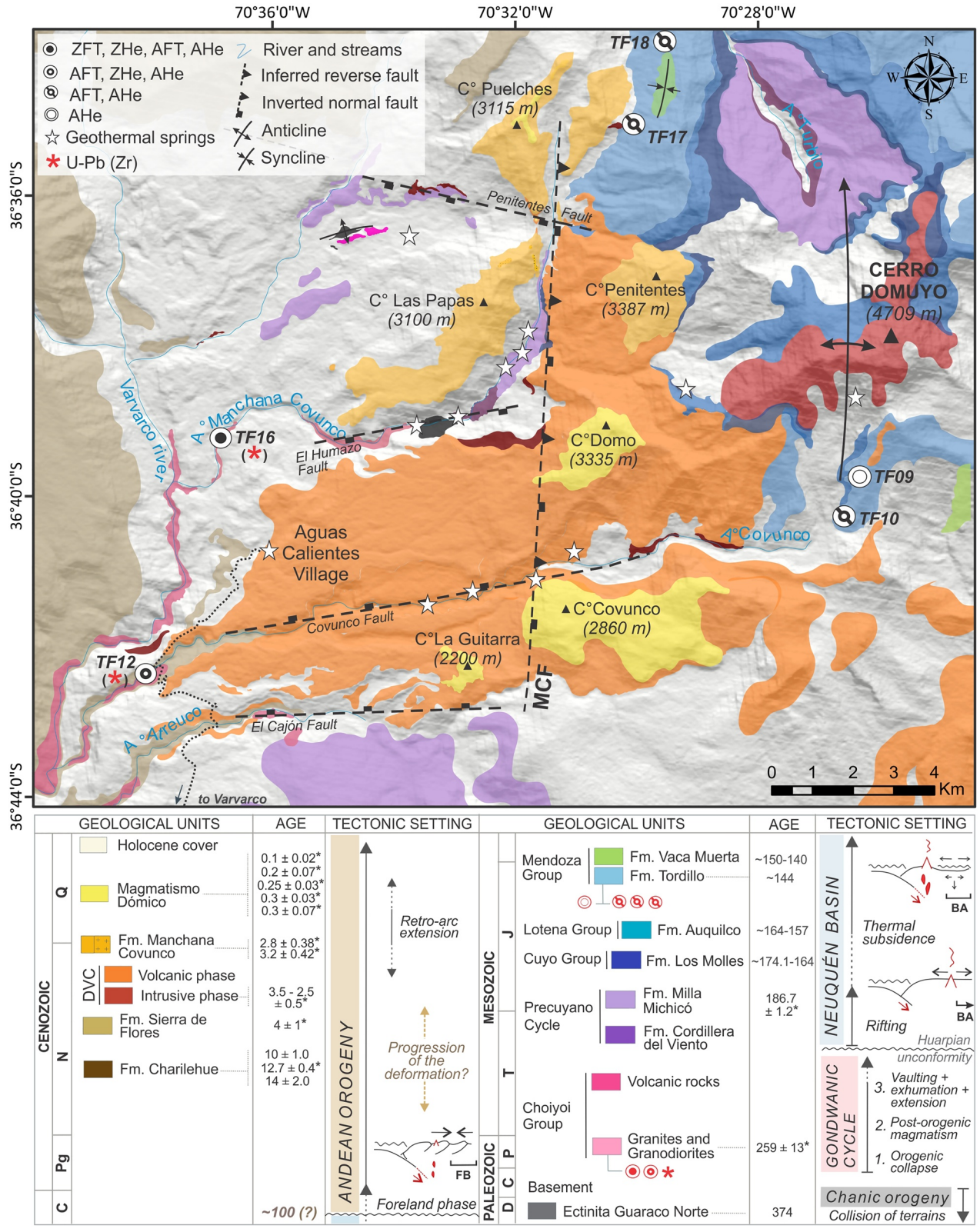

Figure 5. Geological map of the western flank of the Domuyo volcano including the main structures and lithological groups, and the location of analyzed samples (TF09 to TF18). The ages with black asterisks correspond to absolute ages of units exposed in the study area. MCF: Manchana Covunco Fault. BA: back-arc, FB: foreland basin. See Figure 2 for location.

4.2. U-Pb Zircon Geochronology

U-Pb crystallization ages were obtained from two samples from the intrusive rocks of the Choiyoi Group (TF12, TF16; Figure 5), in order to constrain their absolute age and to develop accurate thermal models. Both were previously dated with low-temperature thermochronology techniques. Zircon grains were recovered from the rocks using standard mineral separation techniques, mounted in teflon, and polished. U, Th, and Pb isotopes were analyzed using a Laser Ablation Multi-Collector Inductively Coupled Plasma Mass Spectrometer (LA-MC-ICP-MS) at the Laboratory of Thermochronology La.Te. Andes S.A., Salta, Argentina. The samples were ablated using a RESOlution SE instrument, incorporating a 193 nm ArF excimer laser. The sample cell was flushed with ultrahigh purity He (370 ml min^{-1}) and N_2 (5 ml min^{-1}), both of which were passed through an inline Hg trap. Isotopic signal intensities were measured using an Agilent 8900 triple quadrupole ICP-MS, with high purity Ar as the plasma gas. For sample TF16, the U-Pb analysis was performed on the same zircon crystals previously dated by the ZFT method, plus additional crystals to improve the final concordia age. Data reduction was performed with LADR V.1.1.06 software (Norris & Danyushevsky, 2018). The $^{206}Pb/^{238}U$ ages were used as the preferred age, as they are more precise than $^{207}Pb/^{206}Pb$ for ages younger than 1.2 Ga (Gehrels et al., 2008). The cut-off value for the acceptance and rejection of discordant data has been set to 10%. The weighted mean U-Pb crystallization ages and concordia plots were calculated using the program IsoplotR (Vermeesch, 2018). Procedures and raw data are outlined in detail in the Supporting Information file (S1).

4.3. Zircon and Apatite Fission Track (ZFT-AFT) Analysis

The fission track method is based on the analysis of damage to the crystal lattice—"fission tracks"—that are formed in the mineral structure by the spontaneous fission decay of ^{238}U (Fleischer et al., 1975; Price & Walker, 1963). Retention of the radiogenic daughter product of this decay in the crystalline lattice below a certain temperature range can be modeled using the concept of closure temperature (Tc), above which temperature the system is open and radiogenic decay products are lost through the total shortening of the tracks (Tc: 240 ± 20 °C for ZFT and 100 ± 10 °C for AFT; Brandon et al., 1998; Dodson, 1973; Ketcham et al., 1999; Laslett et al., 1987). Such closure is not instantaneous, and there exists a transitional temperature range, the Partial Annealing Zone (PAZ), in which daughter products are partially lost and partially retained. Consequently, the reduction in the length of the fission tracks depends on the temperature and duration of sample reheating/slow cooling. In nature, significant track shortening occurs within thermal ranges of 60–120 °C for apatites and 200–300 °C for zircons, representing the PAZ for the corresponding mineral (Gleadow & Fitzgerald, 1987; Tagami, 2005). When a rock is subjected to temperatures within the PAZ, the fission tracks become progressively shortened and finally erased, or annealed, by thermal recovery as the crystal lattice damage is repaired (Fleischer et al., 1975).

In this work, fission track cooling ages were obtained from five samples (TF10, TF12, TF16, TF17 and TF18; Figure 5) using the External Detector Method (Hurford & Green, 1983). Ages were calculated using the TrackKey software (Dunkl, 2002). The chi-square test—$P(x^2)$—was applied in each case in order to evaluate data overdispersed in relation to the statistical expectation for the radioactive decay process (Galbraith, 1981; Green, 1981). We measured the kinetic parameter Dpar and confined track lengths (Donelick, 1993; Green et al., 1986). The first consists of the diameter of fission track etch-pits parallel to the apatite crystal *c* axis, and the second of complete fission tracks preserved within the crystal. The length of the confined tracks depends on the amount of shortening experienced during their passage through the PAZ, and on the kinetic characteristics of the crystal, reflected by Dpar (Donelick, 1993; Ketcham et al., 2007). Confined track lengths were corrected using the horizontal angle of the track with respect to the crystallographic *c* axis (Ketcham et al., 2007). See Supporting Information for details of sample preparation and analytical procedures (S2).

4.4. (U-Th-Sm)/He in Zircons and Apatites (ZHe-AHe)

(U-Th-Sm)/He cooling ages are based on the measurement of ^{4}He, which is generated by the radioactive decay of ^{235}U, ^{238}U, ^{232}Th, and ^{147}Sm. Each transformation in the decay chain results in the generation of an energetic particle of ^{4}He. The diffusion of ^{4}He atoms out of the crystal lattice depends fundamentally on the

thermal conditions of the rock sample. In nature, ^{4}He diffusion within the crust occurs within the Partial Retention Zone (PRZ) spanning the temperature interval of ~40–85 °C, with a Tc of 75 ± 5 °C for apatites, and ~130–180 °C with a Tc of 180 ± 10 °C for zircons (Flowers & Farley, 2012, 2013; Flowers et al., 2009; Reiners & Brandon, 2006; Reiners et al., 2004; Wolf et al., 1998). Hence, the ^{4}He generated by radioactive decay within the PRZ is retained within the crystal (Farley, 2000; Wolf et al., 1998). Above the PRZ, ^{4}He escapes from the crystal lattice by means of diffusion, providing cooling ages equal to zero and causing a reset of the isotopic system (Farley, 2000). During the decay process, ^{4}He travels ~20 μm through the crystal lattice before stopping; therefore, some ^{4}He will be ejected from the crystal when the decay occurs within 20 μm of its edges resulting in ages younger than expected (Farley et al., 1996). Radiation may also influence ^{4}He diffusion. The recoil of a parent nuclide of U, Th, or Sm as it decays by ejecting a ^{4}He particle or the formation of a fission track damages the crystal lattice and thereby alters the diffusivity for ^{4}He. In apatites, this can result in older ages than expected; in zircon, very high damage can lead to anomalously young ages (e.g., Flowers et al., 2009; Guenthner et al., 2013).

All the six samples were dated by the AHe technique (TF09, TF10, TF12, TF16, TF17 and TF18), and only two by the ZHe technique (TF12, TF16; Figure 5). A minimum of three single-grain aliquots were dated for intrusive rocks (TF12, TF16), and five for sedimentary samples (TF09, TF10, TF17, TF18). The alpha-ejection correction was applied to account for ^{4}He loss considering the dimensions of each crystal (Farley et al., 1996). See Supporting Information for details of measurement procedures (S3).

4.5. Inverse Thermal History Modeling

Thermal histories were modeled with the QTQt software (Gallagher, 2012) adopting established models to predict fission track annealing and ^{4}He-diffusion kinetics as a function of time and temperature (Farley, 2002; Flowers et al., 2009; Ketcham et al., 2007; Reiners et al., 2004; Tagami et al., 1998). QTQt implements a transdimensional Bayesian Markov Chain Monte Carlo (MCMC) algorithm (Gallagher, 2012; Gallagher et al., 2009) that explores an a priori-defined time-temperature modeling space (general time and temperature priors) in a random walk, along which different thermal paths are proposed, evaluated, and either rejected or accepted. Accepted paths are used to construct the posterior distribution on the thermal history. For AFT data, horizontal confined, and *c* axis projected track lengths were input along with Dpar values as the kinetic parameter (Burtner et al., 1994). All simulations in this study implement the Ketcham et al. (2007) and Tagami et al. (1998) annealing models for fission tracks in apatites/zircons, respectively. For ^{4}He-diffusion kinetics in apatite, we adopted the radiation damage model of Flowers et al. (2009) due to the old stratigraphic age of the samples (~150 Ma for the Tordillo Formation and ~288 Ma for the Choiyoi Group, according to Rossel et al. (2014) and Naipauer et al. (2012, 2015a, 2015b); and to this work, respectively) and to their potential long-term stay near the surface. For ^{4}He-diffusion kinetics in zircon, we applied the radiation damage model of Guenthner et al. (2013). The dimensions and U-Th-Sm and ^{4}He concentrations were input for each zircon/apatite grain. A specific prior of time-temperature ranges and some geological constraints were introduced in the setup for each model. The prior for each model is constrained by the temporal (via input age) and thermal (via thermochronometer) data. The interpretation of the modeled thermal histories and cooling rates estimates are according to the expected (mean) model considering 95% credible intervals (Gallagher, 2012). See Supporting Information for details of methodology, setup, and constraints (S4).

5. Analytical Results

5.1. U-Pb Zircon Crystallization Ages from the Choiyoi Group Rocks

For samples TF12 and TF16, U-Pb zircon ages are presented on two concordia diagrams (Figures 6a and 6c). Analytical results are detailed in the Supporting Information file (Table S1.2). Uncertainties are quoted at the 2σ level for individual analyses, and the error for weighted mean ^{206}Pb/^{238}U ages is quoted at the 2σ (95% confidence) level. The resulting data set presents a narrow range of age values (Figures 6b and 6d). Ages are identical within limits of uncertainties, with weighted mean ages of 288.44 ± 0.70 Ma for sample TF12 and 288.17 ± 0.78 Ma for sample TF16, respectively.

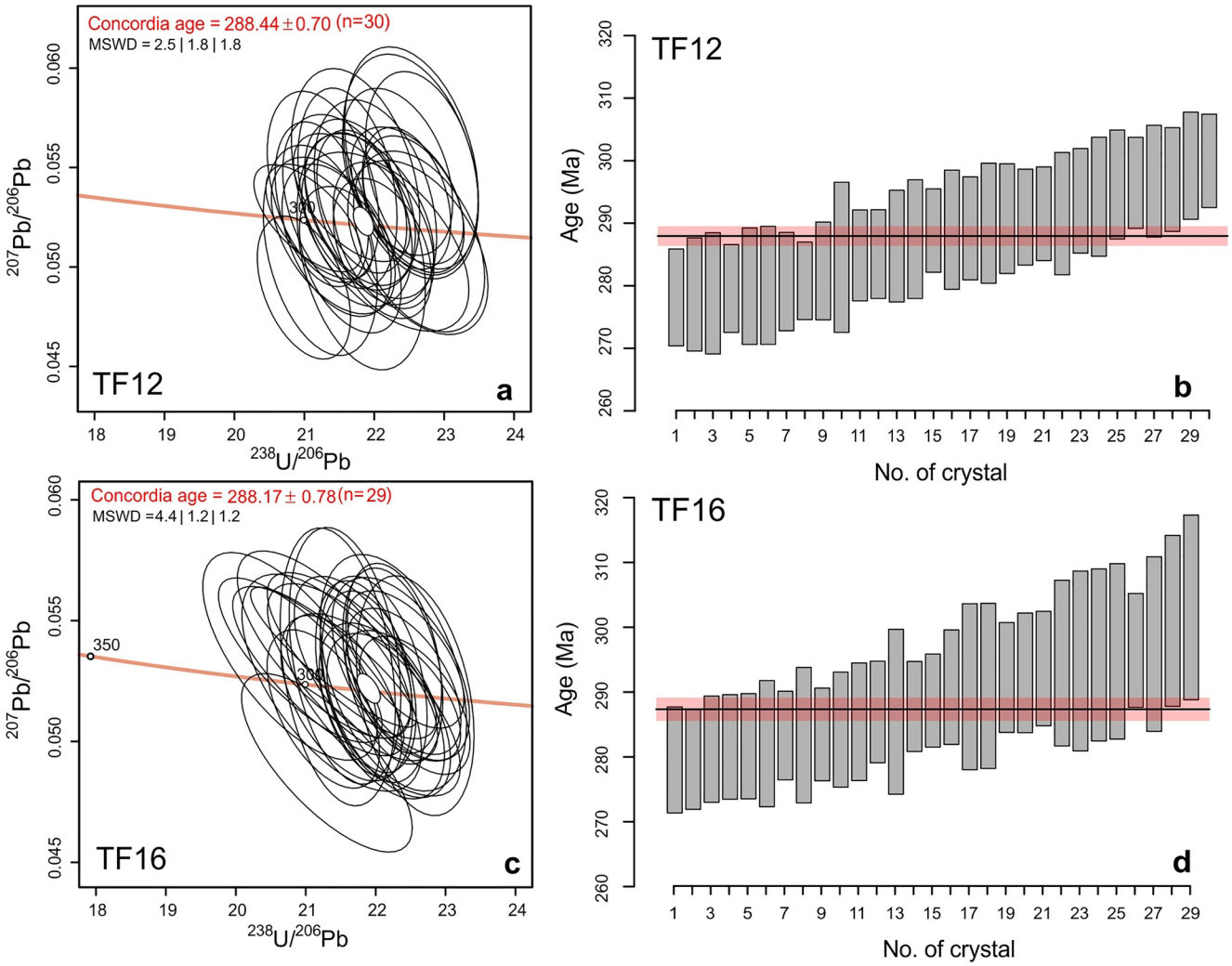

Figure 6. U-Pb results for samples TF12 (a), (b) and TF16 (c), (d) from the Choiyoi Group. (a and c) Concordia ages and Tera-Wasserburg Concordia diagrams calculated using the IsoplotR Software (Vermeesch, 2018). Error ellipses are shown as 2σ. Concordance results and statistical indexes of MSWD (Mean Square Weighted Deviation) are specified as MSWD for concordance | for equivalence | combined for concordance + equivalence. (b and d) Box plots created using the IsoplotR Software (Vermeesch, 2018). Boxes correspond to the $^{206}Pb/^{238}U$ age of each dated zircon-crystal; box height represents the 2σ error.

5.2. Zircon Fission Track (ZFT)

Twenty-eight zircon grains from sample TF16 (Choiyoi Group) yield an Aptian-Albian ZFT central cooling age of 109.9 ± 4.8 Ma (Tables 1 and S2.5). The grain-age distribution has a P(x^2) > 5% consistent with a single population of ages (Galbraith, 1981; Green, 1981) (Figure 7). The same crystals were double dated using the U-Pb technique (Section 5.1, Figure 6, and Table S1.2).

5.3. Apatite Fission Track (AFT)

Samples TF12 and TF16 from the Permian Choiyoi Group yield Late Cretaceous cooling ages of 70.3 ± 5.9 and 84.0 ± 5.8 Ma, respectively. Both of these samples pass the chi-square test (Figure 7). Mean confined track lengths are 13.13 ± 1.79 μm (TF12) and 14.25 ± 1.48 μm (TF16) (Tables 1, S2.5 and S2.6). The low dispersion of grain ages in the radial plots indicate a single population of ages equivalent with P(x^2) values >5%, which is consistent with the low dispersion of confined track lengths and grain ages versus Dpar values (Figure S2.1).

Tectonics

10.1029/2020TC006415

Table 1
Description of the Samples Analyzed and Apatite and Zircon Fission Track Analytical Data

Sample	Latitude (S)	Longitude (W)	Stratigraphic unit	Stratigraphic age	No. of grains	Spontaneous track density $\rho_s \times 10^5$ tracks/cm^2 (Ns)	Induced track density $\rho_i \times 10^6$ tracks/cm^2 (Ni)	Dosimeter track density $\rho_d \times 10^6$ cm^2 (Nd)	Age (Ma) ±1σ	P(x^2)	No. of confined track lengths	Mean of confined track lengths (μm)	Mean track lengths STD (μm)	Mean Dpar (μm)
TF09	36°40′23″	70°26′36″	Tordillo Fm.	Upper Jurassic	*x*	*x*	*x*	*x*	*x*	*x*	*x*	*x*	*x*	*x*
TF10	36°40′47.8″	70°26′46.3″	Tordillo Fm.	Upper Jurassic	41 (Ap)	0.95 (115)	0.53 (634)	1.07 (6,713)	33.2 ± 3.5	96	2	12.44	0.63	2.8
*TF12	36°42′20.8″	70°38′1.4″	Choiyoi Group	Permian	33 (Ap)	8.46 (655)	2.02 (1,561)	0.97 (5,372)	70.3 ± 5.9	31	73	13.13	1.79	1.7
*TF16	36°39′10.6″	70°36′48.3″	Choiyoi Group	Permian	24 (Ap)	10.04 (1,208)	1.23 (1,481)	0.63 (4,866)	84.0 ± 5.8	12	71	14.25	1.48	1.6
					28 (Zr)	193.24 (9,747)	48.77 (2,460)	5.22 (5,000)	109.9 ± 4.8	36	—	—	—	—
TF17	36°35′17.5″	70°30′18.1″	Tordillo Fm.	Upper Jurassic	44 (Ap)	2.87 (259)	1.13 (1,021)	1.05 (6,546)	45.5 ± 3.5	90	7	13.86	1.34	1.9
TF18	36°33′55.2″	70°29′31.7″	Tordillo Fm.	Upper Jurassic	24 (Ap)	1.89 (118)	0.87 (545)	1.04 (6,504)	38.5 ± 4.1	84	3	14.51	0.20	2.1

Note. Abbreviations are Ns, total number of spontaneous tracks; Ni and Nd, total numbers of induced and dosimeter tracks; P(x^2), x^2 probability. Mean of confined track lengths are corrected using its horizontal angle with respect to the *c* axis of the crystal. ζ zeta value: 107.3 ± 3.6 (ZFT_TF16); 331.2 ± 17.0 (AFT_TF16); 344.1 ± 22.1 (AFT_TF12); 342.9 ± 8.7 (AFT_10-17-18). Counted by Dr. Arzadún G. from La.Te. Andes S.A. (ZFT_TF16) and Dr. Galetto A. (rest of the samples). Etching conditions: 5 N (HNO_3) for 21 s at 21 °C (AFT_10-17-18); 5.5 N (HNO_3) for 20 s at 20 °C (AFT_12-16); NaOH-KOH eutectic solution of 8 g of sodium hydroxide (NaOH) and 11.5 g of potassium hydroxide (KOH), melted at 210 °C (ZFT_TF16). Dosimeter glasses: CN5 with 12.5 ppm of U (AFT_10-17-18); IRMM540 glass (AFT_TF12-16); and IRMM541 (ZFT_TF16). Samples with asterisks correspond to those also dated through U-Pb in zircon technique. See the Supporting Information (S2) for more information.

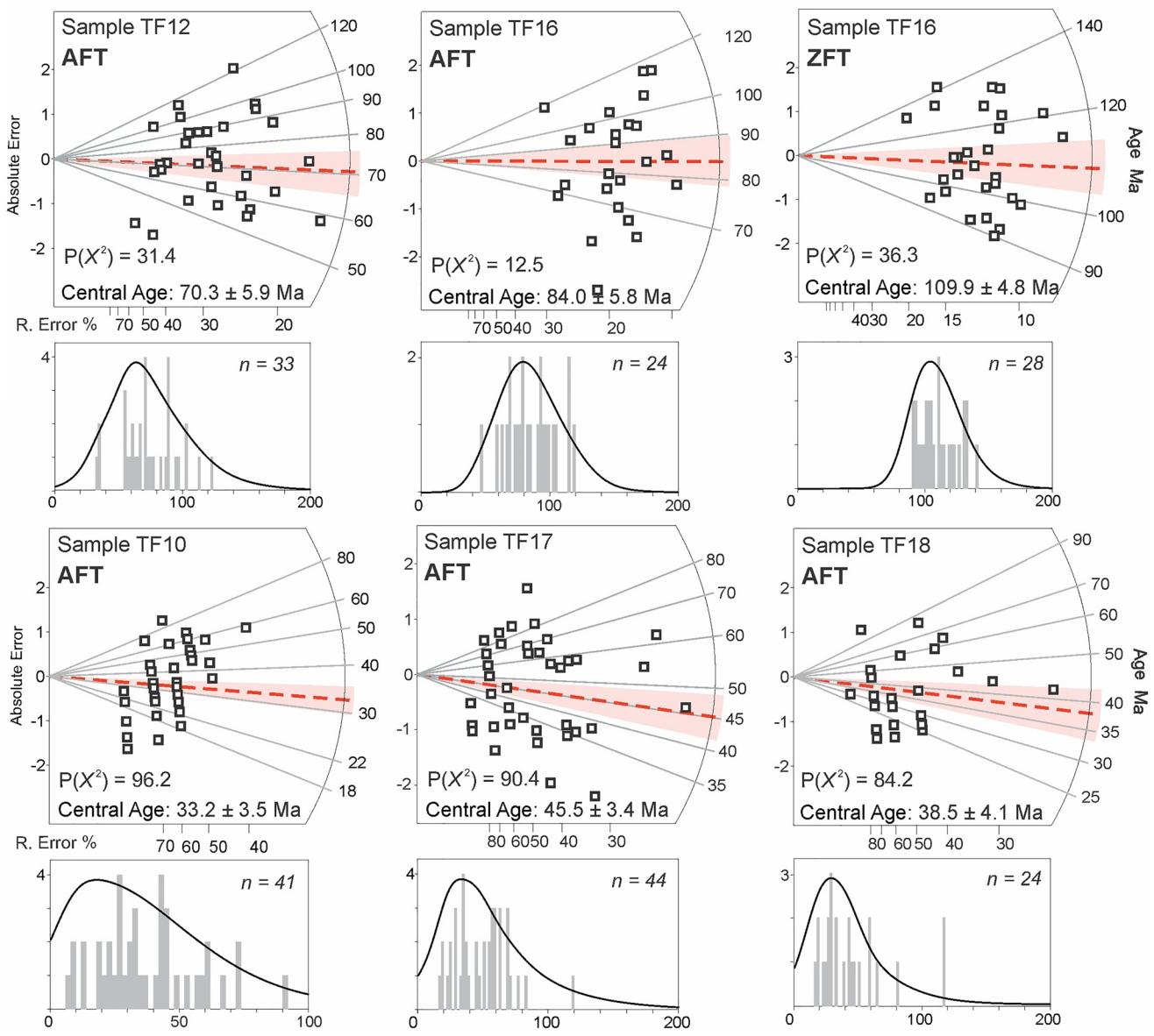

Figure 7. Radial plots showing the distribution of fission track ages. Plots show the relative error versus absolute error (above) and frequency histograms (below), constructed using TrackKey software (Dunkl, 2002) for each sample analyzed by AFT and ZFT. TF10, TF17, and TF18: Tordillo Formation; TF12 and TF16: Choiyoi Group. *n*: total number of analyzed crystals. Central ages and their range of analytical uncertainty are represented with red dashed lines and red shadowed areas, respectively.

The sedimentary samples from the Upper Jurassic Tordillo Formation (TF10, TF17, and TF18), located east of the MCF (Figure 5), yield Paleogene cooling ages. The central ages are 45.5 ± 3.5 Ma (TF17), 38.5 ± 4.1 Ma (TF18), and 33.2 ± 3.5 Ma (TF10). All samples have been completely reset prior to exhumation, as indicated by grain-age distributions with P(x^2) > 5% (Figure 7). Only a small number of confined tracks lengths could be measured (Tables 1, S2.5 and S2.6).

5.4. (U-Th-Sm)/He in Zircons (ZHe)

Three ZHe single-grain aliquots were processed from each of the Choiyoi Group samples. Late Cretaceous single-grain cooling ages range from 65.3 ± 0.4 to 78.2 ± 0.4 Ma for TF12, and from 65.7 ± 0.8 to 84.8 ± 0.8 Ma for TF16 (Table 2).

5.5. (U-Th-Sm)/He in Apatites (AHe)

Three AHe single-grain aliquots were processed from each of the Choiyoi Group samples. Eocene single-grain cooling ages range from 41.3 ± 0.5 to 56.1 ± 0.7 Ma with a weighted mean age of 47.8 ± 6.1 Ma for TF16, and from 46.1 ± 1.0 to 56.2 ± 0.9 Ma with a weighted mean age of 49.6 ± 4.4 Ma for TF12 (Table 2). The errors of reported weighted mean ages correspond to the standard deviation of single-grain ages.

Table 2
(U-Th-Sm)/He Analytical Data

Grain no.	Raw age (Ma)	±σ (Ma)	ESR (μm)	U (ppm)	Th (ppm)	Sm (ppm)	$Th/^{238}U$	^{4}He (nmol/g)	eU (ppm)	FT	Crystal terminations	FT correct. age (Ma)	1σ (Ma)
(U-Th-Sm)/He in zircons													
TF_12_Zr1	53.9	0.3	70.8	365.2	140.5	0.4	0.4	116.2	398.2	0.82	2	65.3	0.4
TF_12_Zr2	55.0	0.2	57.8	450.1	181.8	0.2	0.4	146.8	492.8	0.79	2	69.9	0.3
TF_12_Zr3	63.0	0.3	63.8	261.4	137.2	0.5	0.5	100.4	293.6	0.80	2	78.2	0.4
TF_16_Zr1	64.1	0.6	50.4	215.3	174.2	0.4	0.8	89.1	256.2	0.75	2	84.8	0.8
TF_16_Zr2	55.6	0.5	40.5	314.9	206.4	0.6	0.7	109.6	363.4	0.70	2	79.3	0.7
TF_16_Zr3	49.7	0.6	50.2	581.4	290.6	1.3	0.5	174.8	649.7	0.76	2	65.7	0.8
(U-Th-Sm)/He in apatites													
TF_09_Ap1	0.7	0.1	33.2	10.8	132.5	2159.4	12.5	0.2	42.0	0.59	1	1.2	0.1
TF_09_Ap2	1.7	0.4	29.4	3.5	15.5	93.5	4.6	0.1	7.1	0.55	2	3.2	0.7
TF_09_Ap3	0.8	0.2	33.4	4.7	14.9	201.9	3.3	0.0	8.2	0.59	0	1.4	0.4
TF_09_Ap4	0.9	0.3	22.4	7.0	22.4	1171.3	3.3	0.1	12.2	0.43	2	2.0	0.7
TF_09_Ap5	2.6	1.1	22.1	2.4	4.2	7.6	1.8	0.1	3.4	0.43	2	6.3	2.6
TF_10_Ap1	2.3	0.1	47.3	4.8	23.5	213.2	5.1	0.1	10.3	0.70	1	3.4	0.2
TF_10_Ap2	2.6	0.2	42.9	4.5	24.5	200.1	5.6	0.2	10.3	0.67	2	5.0	0.2
TF_10_Ap3	6.0	0.3	32.3	7.8	32.8	269.7	4.3	0.5	15.5	0.58	2	10.7	0.5
TF_10_Ap4	1.3	0.1	42.5	10.2	47.4	296.8	4.8	0.2	21.3	0.67	0	2.0	0.2
TF_10_Ap5	4.3	0.3	41.5	2.8	14.0	163.6	5.1	0.2	6.1	0.67	2	6.6	0.5
TF_12_Ap1	45.1	0.7	75.5	11.2	19.6	20.5	1.8	3.9	15.8	0.80	2	56.2	0.9
TF_12_Ap2	34.7	0.5	54.2	26.5	60.6	40.6	2.4	7.7	40.8	0.72	2	47.9	0.7
TF_12_Ap3	29.3	0.6	41.1	22.7	46.6	44.6	2.1	5.4	33.6	0.64	2	46.1	1.0
TF_16_Ap1	43.2	0.5	65.3	39.3	68.7	320.1	1.8	13.1	55.5	0.78	2	56.1	0.7
TF_16_Ap2	38.1	0.5	60.9	27.1	45.3	401.4	1.7	7.9	37.7	0.76	2	50.3	0.6
TF_16_Ap3	31.6	0.4	63.6	33.2	55.0	401.1	1.7	8.0	46.1	0.77	1	41.3	0.5
TF_17_Ap1	22.7	0.3	31.1	70.2	85.6	307.3	1.3	11.1	90.3	0.57	2	40.8	0.6
TF_17_Ap2	11.8	1.2	36.0	5.4	21.9	231.6	4.2	0.7	10.6	0.62	1	19.6	1.9
TF_17_Ap3	29.6	0.5	41.0	40.3	5.4	132.2	0.1	6.7	41.6	0.66	2	45.0	0.7
TF_17_Ap4	6.2	0.5	33.8	2.5	11.5	54.9	4.7	0.2	5.2	0.60	2	10.8	0.8
TF_17_Ap5	22.3	0.6	35.4	15.7	6.6	253.8	0.4	2.1	17.2	0.61	1	36.3	1.0
TF_18_Ap1	17.3	0.7	35.2	5.4	22.4	135.6	4.3	1.0	10.6	0.61	2	29.3	1.2
TF_18_Ap2	28.5	0.6	36.3	6.0	19.3	138.0	3.3	1.7	10.5	0.62	1	47.2	1.0
TF_18_Ap3	25.1	0.5	46.4	4.6	15.4	155.7	3.4	1.2	8.2	0.70	0	36.8	0.7
TF_18_Ap4	18.9	0.7	32.8	6.0	37.9	207.7	6.4	1.6	15.0	0.59	2	33.7	1.2
TF_18_Ap5	15.6	0.9	33.8	2.7	9.9	185.4	3.7	0.5	5.1	0.60	1	26.6	1.6

Note. Weighted mean errors are reported. See the Supporting Information for details (S3).

Two samples from the Tordillo Formation collected east of the Manchana Covunco fault and along the northern flank of the Domuyo volcano were dated with AHe (TF17 and TF18; Figure 5). Five AHe single-grain aliquots per sample provided single-grain ages between 10.8 ± 0.8 and 45.0 ± 0.7 Ma for TF17, and between 26.6 ± 1.6 and 47.2 ± 1.0 Ma for TF18. Corrected AHe ages (to account for ^{4}He loss considering the dimensions of each crystal; Farley et al., 1996) show a positive correlation with effective uranium content (eU) (Figure S3.1). The other two samples from the Tordillo Formation collected along the southern flank of the Domuyo volcano (TF09 and TF10; Figure 5) yield AHe ages ranging between 1.2 ± 0.1 Ma and 6.3 ± 2.6 Ma for TF09, and between 2.0 ± 0.2 and 10.7 ± 0.5 Ma for TF10 (Table 2). Two of the measured grains from sample TF09 are rather small (FT correction factor of 0.4) and should be interpreted with caution. The entire data set lacks a correlation between grain size and cooling ages (Figure S3.1).

6. Modeling Results

Thermal history modeling was performed on data from Paleozoic basement and Mesozoic sedimentary samples, from the western and eastern blocks of the Manchana Covunco fault (MCF), respectively. Details about the model setup are provided in the Supporting Information (S4).

6.1. Western Block of MCF: Thermal Histories of Choiyoi Group Samples

Inverse thermal history modeling was performed on Choiyoi Group intrusive samples (TF12, TF16) by combining ZFT, ZHe, AFT, AHe data, and >70 confined track lengths for each sample. The obtained Permian U-Pb crystallization ages of 288.44 ± 0.70 Ma (TF12) and 288.17 ± 0.78 Ma (TF16) for Choiyoi Group samples (Figure 6 and Table S1.2) and the Middle-Upper Triassic Huarpic erosion surface (Azcuy & Caminos, 1987; Llambías et al., 2007, 2011) were introduced as geological constraints for the models. See Supporting Information for more details about constraints (S4).

The data input for sample TF12 included 33 single-grain AFT ages (with grain-specific mean Dpar values), with 73 horizontal confined track lengths, 3 AHe and 3 ZHe single-grain ages (Tables 1 and 2, S2.5 and S2.6). The modeling output shows a well-constrained thermal history with good fits to the observed data (Figure 8a). The expected model matches the observed AFT age. The AHe predictions cluster around the two younger single-grain ages (~35–30 Ma), whereas the oldest AHe age is underpredicted (younger than observed), but still within the range of analytical uncertainty. The ZHe predictions cluster around the oldest ZHe single-grain age (~65 Ma) and overpredict two younger ages within the range of analytical uncertainty. Two abrupt pulses of rapid cooling are predicted between ~90–75 Ma and ~55–30 Ma in a stepwise fashion, separated by a protracted residence in the AFT PAZ at ~90–100 °C. The residence of the sample within the PAZ temperatures is coherent with the observed minor group of shorter confined track lengths within this sample.

For sample TF16, the model input consisted in ZFT ages from 28 zircon crystals, AFT ages from 24 apatites with grain-specific mean Dpar values and 71 horizontal confined track lengths, as well as 3 AHe and 3 ZHe single-grain ages (Tables 1 and 2, S2.5 and S2.6). This sample was modeled as two different samples (4 m vertical offset) in order to combine both AFT and ZFT data sets. This procedure is required by the QTQt program. The modeling output constrains the onset of the first episode of rapid cooling as between 110 and 100 Ma (Figure 8b). In this thermal history, cooling rates abruptly decelerate after ~75 Ma and remain slow throughout the PAZ. This change is almost coeval with the end of TF12 first cooling pulse. Since then, cooling rates remain slow and constant until reaching surface conditions. Predicted AFT ages, confined track lengths distribution, and ZHe and AHe ages are consistent with the observed data. The expected model (mean model from all sampled thermal histories) significantly overpredicts the observed ZFT data; however, the maximum likelihood model predicts these data well and is very similar in shape to the mean (expected) thermal history. For more details and extended modeling results see Supporting Information (S4).

6.2. Eastern Block of MCF: Thermal Histories of Tordillo Formation Samples

The Tordillo Formation samples were modeled through the combination of AFT and AHe data. Few confined track lengths were included in each case ($n < 7$), without significant impact on the model outputs. A

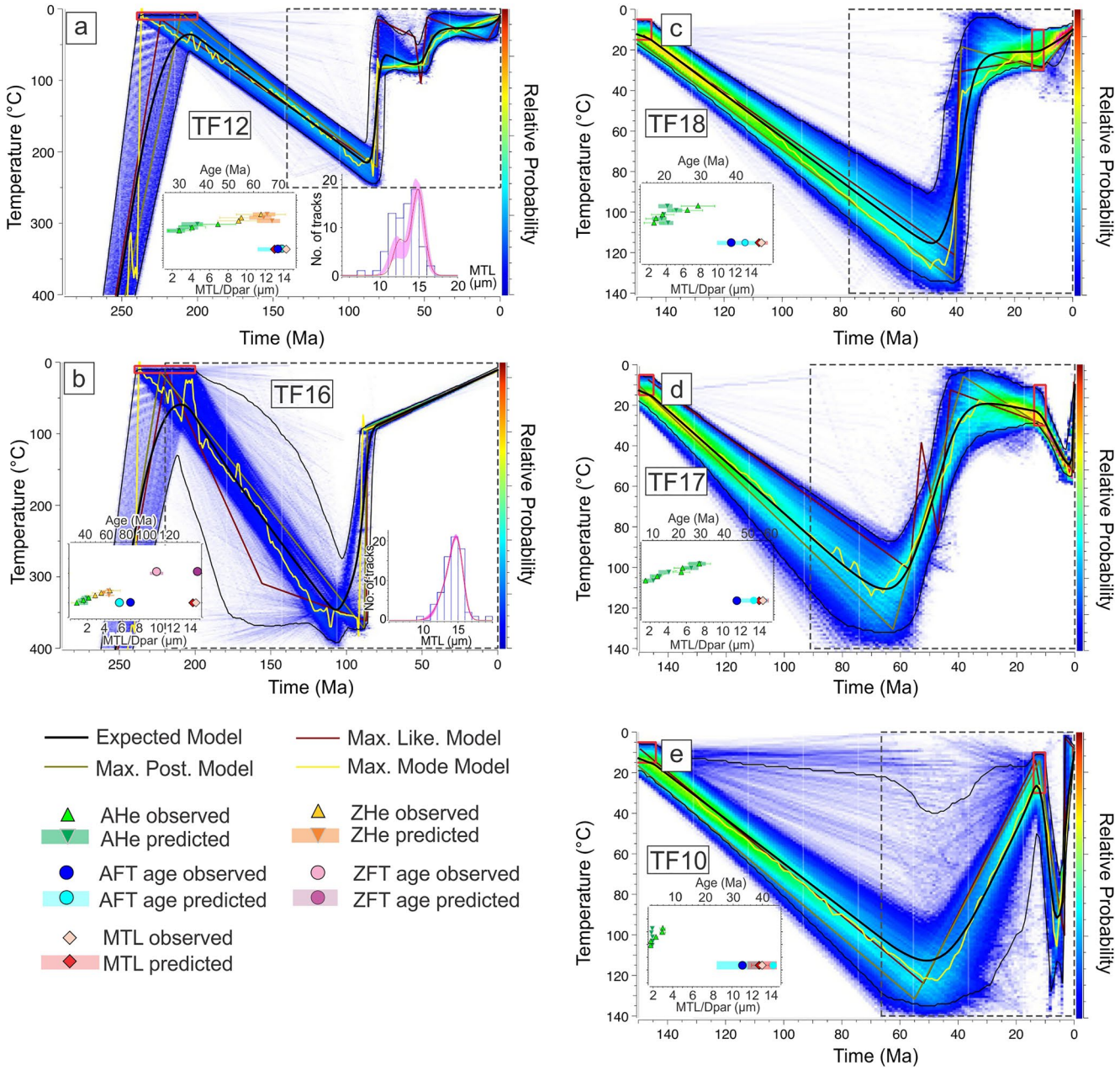

Figure 8. QTQt modeling results for igneous (Choiyoi Group: TF12, TF16; 8a, b) and sedimentary (Tordillo Formation: TF18, TF17, TF10; 8c, d, e) samples. Inset plots present predicted versus observed ages/MTL plotted against sample elevation (default minor offset between aliquots for the sake of clarity). All predicted versus observed data correspond to the expected (average) model generated by QTQt (black lines representing the mean and 95% confidence intervals for the average thermal history). The predictions from the maximum likelihood models (very similar to the expected model) are given in the Supporting Information (Figure S4.1) (e.g., Gallagher, 2012; Gallagher & Ketcham, 2020). The green (AHe), orange (ZHe), cyan (AFT), red (mean track length), and violet (ZFT) bands represent the 95% credible intervals for the predictions (sampled intervals).

Late Jurassic depositional age (Naipauer et al., 2012, 2015a, 2015b; Rossel et al., 2014) and a local middle Miocene angular unconformity (Folguera et al., 2007; Silva et al., 2018) were introduced as geological constraints for the models. See Supporting Information for more details about constraints (S4).

For sample TF18, the model input included AFT ages from 24 apatites with grain-specific mean Dpar values and 3 horizontal confined track lengths, as well as 5 AHe single-grain ages (Tables 1 and 2, S2.5 and S2.6). The modeled thermal histories are well-constrained, matching most of the observed data (except the oldest

AHe age) within the range of analytical uncertainty (Figure 8c). The modeled thermal history indicates a major pulse of rapid cooling (~100 °C) reaching near-surface temperatures and starting between 50 and 40 Ma, roughly coinciding with the younger cooling event recorded by the thermal history of TF12.

For sample TF17, thermal histories were performed with 44 AFT grain ages with grain-specific mean Dpar values and 7 horizontal confined track lengths, as well as 5 AHe single-grain ages (Tables 1 and 2, S2.5 and S2.6). The obtained thermal model reflects a similar rapid cooling event constrained between 65-55 and 40-35 Ma (Figure 8d). After 40 Ma, the thermal path marks a residence at near-surface temperatures (~20 °C) or slow reheating until ~15-10 Ma, followed by an abrupt reheating to >50 °C and very recent cooling until surface conditions. The later event likely induced a partial reset of AHe ages as evidenced by the dispersion of their ages (Table 2).

The single-grain ages for both TF17 and TF18 samples are excellently predicted by the expected models (Figures 8c and 8d). Notably, AHe single-grain ages show a positive correlation with eU (effective uranium) values for both samples (Figure S3.1), suggesting some degree of accumulated radiation damage likely influenced ^{4}He-diffusion of apatite grains, and is therefore responsible for the observed dispersion of AHe cooling ages.

Finally, sample TF10 was modeled with 41 AFT ages with grain-specific mean Dpar values, 2 confined track lengths, as well as 5 AHe single-grain ages (Tables 1 and 2, S2.5 and S2.6). The expected model predicts the observed data within the range of analytical uncertainty, except for the two oldest AHe ages (Figure 8e). A pulse of rapid cooling is predicted at ~50 Ma, closely mimicking those recorded for samples TF17 and TF18, but less constrained in terms of temperature range. After 15-10 Ma, an abrupt reheating to >80 °C is responsible for the total resetting of all AHe ages and followed by very recent accelerated cooling to surface temperatures. The modeled thermal histories underpredict the two oldest AHe ages, which might be due to partial resetting of these grains or possible flaws during grain selection. There is no clear correlation between cooling ages and eU-values for this sample (Figure S3.1).

The young (<10 Ma) reheating event predicted by TF17 and TF10 thermal histories has likely affected the TF09 sample as reflected by the very young (fully reset) AHe cooling ages of this sample (Table 2).

7. Discussion and Tectonic Implications

The modeled thermal histories constrain different heating and cooling events during the time-temperature evolution of the Domuyo area. In the following, these are chronologically discussed and integrated in the framework of the regional tectonic scenarios, including the implications for exhumation-cooling mechanisms and their relationship with the MCF, and the final thermal effect of DVC on the cooling history.

7.1. Chronological Development of Reheating, Deformation, and Exhumation in the Domuyo Area

7.1.1. Neuquén Basin Development. Resetting of Fission Track and (U-Th-Sm)/He Ages

The uniform distribution of Dpar and confined track lengths versus grain ages of the Choiyoi Group and Tordillo Formation is consistent with corresponding P(x^2) values >5% and the presence of a single population of ages (Table 1; Figures 7 and S2.1). These characteristics together with the fact that the obtained cooling ages are much younger than their depositional and/or U-Pb crystallization ages (Figure 6) imply that the fission track and (U-Th-Sm)/He isotopic systems were totally reset.

Progressive reheating related to the opening, subsidence, and filling of the Neuquén Basin in a wide-rift setting as well as significant volcanic activity and crustal extension are the main processes responsible for the total reset of both isotopic systems (Franzese & Spalletti, 2001; Franzese et al., 2003) (stages 2B and 2A in Figure 9c and Figures 10a and 10b). The rift stage is evidenced by N-S and W-NW striking normal faults in the Domuyo and Cordillera del Viento areas (Galetto et al., 2018; Sagripanti et al., 2014). The total reset of the AFT and AHe systems in the Tordillo Formation indicates progressive subsidence and burial above the AFT closure temperature (110 ± 10 °C) with a thermal peak around 130 °C (Figures 8c, 8d, 8e, and 9c). The maximum temperature of 130 °C is consistent with burial depths of >2.6 km according to a geothermal

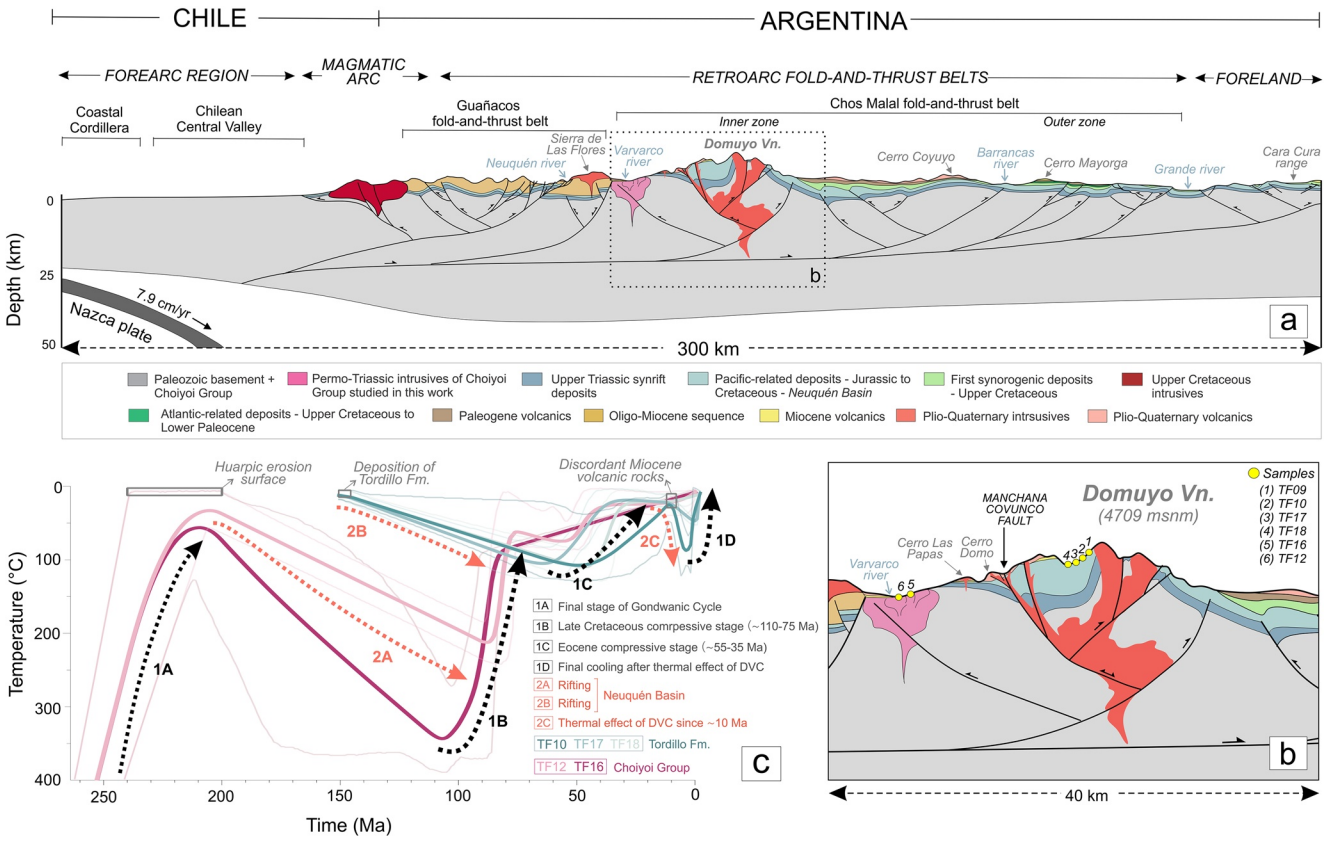

Figure 9. (a) Schematic structural profile across the main morphostructural units at 36°30′S, modified from Zamora Valcarce et al. (2009), Orts et al. (2012), Rojas Vera et al. (2014a, 2014b), Folguera et al. (2015), Sánchez et al. (2018), Turienzo et al. (2018), and Colavitto et al. (2019). (b) Generalized structural profile of the Domuyo area. The location of samples is projected onto the profile maintaining their relative elevation. See Figure 5 and Table 1 for locations and coordinates. (c) Compilation of the expected (average) model generated by QTQt from Choiyoi Group and Tordillo Formation samples (Figure 8). Dark/light pink lines correspond to the Choiyoi Group and dark/light blue to the Tordillo Formation. In each case, thick lines are the mean model and thin lines represent the 95% confidence intervals for each average thermal history. Black dotted arrows correspond to different cooling phases and red dotted arrows to heating/reheating phases. Gray boxes represent geological constraints introduced in the models.

gradient of ~51 °C/km. This latter estimate corresponds to the modern easternmost region of the Neuquén Basin (Sigismondi, 2013; Sigismondi & Ramos, 2009a, 2009b), which was not affected by Andean deformation and can be considered an analogue to the pre-Andean tectonic scenario of the study area. This burial depth is in good agreement with those estimated by Galetto et al. (2018) east of the MCF; with paleo-depths of >4.2-2.3 km interpreted for the southeastern flank of Domuyo volcano (Folguera et al., 2015), and with the deposition of 3–3.6 km of Mesozoic sedimentary rocks east of Cordillera del Viento since Late Jurassic times (Sánchez et al., 2018). The estimated burial depth could be even higher considering the high subsidence rates estimated for the Tordillo Formation in southern Mendoza province (Mescua et al., 2020).

7.1.2. Cretaceous Cooling Period (Albian-Campanian)

The oldest cooling age and the thermal histories of Choiyoi Group samples reflect and Albian-Campanian cooling episode, lasting since ~110 to 75 Ma (Table 1, Figures 8a, 8b, and 10c, and stage 1B in Figure 9c). This cooling episode is consistent with: (i) the onset of the Andean orogeny interpreted by provenance studies in the foreland of the Southern Andes between 34°S and 39°S (Balgord & Carrapa, 2016; Borghi et al., 2019; Di Giulio et al., 2012, 2016; Gómez et al., 2019; Tunik et al., 2010) (Figures 2 and 3); (ii) the beginning of exhumation and magmatism in the fore-arc (Glodny et al., 2008; Tapia et al., 2020); and (iii) a major change in plate's configuration and spreading rates at a global scale (Matthews et al., 2012; Müller et al., 2016; Somoza & Zaffarana, 2008). Assuming the geothermal gradient of ~51 °C/km (Sigismondi, 2013; Sigismondi & Ramos, 2009a, 2009b), the Albian-Campanian rapid cooling event implies maximum cooling rates of 12 ± 4 to 23 ± 10 °C/Ma and exhumation rates of up to ~0.5 ± 0.2 mm/yr (see Table S4.2 for de-

tails about calculation). This phase of the thermal history represents the earliest tectonically driven cooling event recognized in the ChMFTB, and can be precisely correlated with the maximum depositional ages of ~109–100 Ma for the first synorogenic deposits in the Neuquén Basin, represented by the Neuquén Group (Borghi et al., 2019; Di Giulio et al., 2012, 2016; Fennell et al., 2015; Gómez et al., 2019; Tunik et al., 2010, Figures 2 and 4). These deposits register >1,500 m of sedimentary rocks in some sectors of the basin (Legarreta & Uliana, 1999), and between 250 and 550 m in its northern part at 34°–36°S (Borghi et al., 2019; Gómez et al., 2019; Mescua et al., 2013; Orts et al., 2012). Moreover, the sedimentary evidence at 36°–37°S indicates >2,500 m of denudation driven by the Late Cretaceous contractional phase of the Southern Central Andes, shaping the mountain system with a topographic front defined by the Cordillera del Viento anticline between 70°00′W and 70°30′W (present coordinates) (Borghi et al., 2019, Figure 2). This is consistent with Paleogene volcanic rocks that rest in angular unconformity on top of the deformed basement and Choiyoi Group units in the western foothills of the Cordillera del Viento, indicating significant contraction before Paleogene times (Jordan et al., 2001). This phase of orogenic construction is equivalent to the Peruvian orogenic phase defined by Steinmann (1929) further north in the northern segment of the Central Andes. To the south, it is synchronous with the onset of Late Cretaceous mountain building in the Patagonian Andes (Echaurren et al., 2016; Fosdick et al., 2011; Genge et al., 2021; Ghiglione et al., 2014; Gianni et al., 2018; Klepeis et al., 2010; Savignano et al., 2016; Thomson et al., 2001, 2010; among others).

Importantly, the lack of correlation between most of the previously published cooling ages and the maximum depositional ages of the Neuquén Group at these latitudes is probably because most of the thermochronological data are from Mesozoic sedimentary units of the eastern sectors of the basin (Figure 2). Such samples usually yield nonreset or partially reset fission track and (U-Th-Sm)/He ages, as their burial depths are not enough to fully reset these isotopic systems. In the case of Mesozoic nonreset sedimentary samples, cooling ages only provide old (pre-Andean) thermal information from their provenance areas; whereas in the case of partially reset samples only the youngest Cenozoic grain-age populations likely reflect reliable local cooling episodes associated to the final stages of the Andean orogeny (Folguera et al., 2015; Sánchez et al., 2018; Zamora Valcarce et al., 2009). Therefore, the early stages of the Andean cooling/exhumation have remained poorly constrained by the fission track and (U-Th-Sm)/He cooling signals of these sedimentary rocks.

7.1.3. Paleocene Orogenic Quiescence

Since the end of the Campanian, thermal histories of the Choiyoi Group exhibit a progressive decrease in the cooling rates along different trajectories toward surface temperatures (Figure 9c). The TF16 model indicates uniform slow cooling rates until the present (Figure 8b), whereas the TF12 expected model reflects protracted cooling through the apatite PAZ between 75 and 55 Ma (Figure 8a). These thermal histories likely reflect a period of orogenic quiescence matching diverse tectonic settings proposed for this period at 37°S: (i) a potential postorogenic relaxation stage that followed the initial uplift of the Andes (Llambías & Aragón, 2011); (ii) an extensional tectonic episode in response to a southward spread mid-oceanic ridge subduction between ~35°S and 37°S (Fennell et al., 2019; Iannelli et al., 2020). Synchronously, the paraconformable deposition of the Malargüe Group deposits, including the first Atlantic-related marine succession on top of Neuquén Basin deposits (Figures 2 and 4), implies a mild and widespread subsidence in the retro-arc and foreland areas, which is also consistent with a relative quiescence stage and slow rates of sediment accumulation (Aguirre-Urreta et al., 2010; Fuentes & Horton, 2020). At a global scale, the low cooling rates between 75 and 55 Ma precisely match a plate motion global event defined by a major drop in relative spreading rates around 70 Ma between Africa and South American plates, followed by a gradual acceleration in rates after ~55-50 Ma (Colli et al., 2014; Müller et al., 2016).

7.1.4. Eocene Cooling Period

The modeled thermal histories for the Tordillo Formation (Figures 8c–8e) indicate rapid Eocene cooling (~55-35 Ma, stage 1C in Figures 9c and 10d) matching the youngest cooling episode predicted for the Choiyoi Group TF12 sample (Figures 8a and 9c). This episode is associated with maximum cooling rates of 5.8 ± 1.2 °C/Ma (see Table S4.2 for further details). The available confined track lengths for the Tordillo Formation samples are scarce ($n \leq 7$) (Table 1); however, the consistency of the first cooling episode predicted by all Tordillo thermal histories, and their similar AFT and AHe ages, suggest that rapid cooling was triggered by accelerated exhumation that we suggest is associated with an important deformational event.

This episode represents a distinct and specific orogenic event preceded by a relative orogenic quiescence (TF12), contrary to the previously proposed rather continuous "Late Cretaceous-Paleogene" constructional period described in the ChMFTB (Folguera et al., 2015; Rojas Vera et al., 2015; Sánchez et al., 2018, 2020).

Importantly, the Eocene exhumational stage recognized in the study area is synchronous with a remarkable angular unconformity carved over Paleogene rocks of the Malargüe Group and recorded east and southeast of the Domuyo area between ~36°S and 37°S, with a likely southward declining angularity, supporting a phase of tectonism in the Andes and foreland basin at this time (Orts et al., 2012; Ramos, 1981; Rodríguez et al., 2011; Sagripanti et al., 2011, 2012, Figure 4). The unconformity marks the limit between the Eocene strata of the upper Malargüe Group and upper Oligocene to lower Miocene volcanoclastic deposits, indicating the existence of a late Eocene uplift in the region, older than ~30 Ma (Orts et al., 2012; Ramos, 1981; Rodriguez et al., 2011; Sagripanti et al., 2011, 2012).

Notably, the distribution of synorogenic deposits linked to the Eocene orogenic phase at 36°–37°S is still under discussion. Volumes of these deposits are low north of the Cortaderas lineament and even more limited to the south (Ramos & Kay, 2006). In southern Mendoza province (36°25′S), a 50–100-m thick synorogenic sequence attributed to the upper Malargüe Group strata has been recognized, which contains sandstones and conglomerates deposited during a progressive continentalization and progradation of fluvial systems to the southeast following the regression of the Atlantic Ocean (Kozlowski et al., 1987; Sagripanti et al., 2012).

Whether contemporaneous foreland basin strata support major deformation in the Eocene remains an open question, evidence for changes in the tectonic regime at ca. 49 Ma in the ChMFTB derives from an eastward migration of the volcanic arc (Cobbold & Rossello, 2003; Cobbold et al., 1999; Kay et al., 2006). The cessation of Paleogene volcanism west of the Cordillera del Viento and its initiation to the east has been attributed to an eastward shift of the volcanic front during Eocene times, accompanied by contractional deformation (Kay et al., 2006). Moreover, an Eocene compressive event east of Cordillera del Viento has been postulated by Cobbold et al. (1999), based on contractional structures, orientation of bitumen veins cross-cutting deformed Cretaceous strata, and ages of magmatic rocks in Huantraico syncline (Cobbold & Rossello, 2003).

At a regional scale, the Eocene compressive stage corresponds to the southward continuation of the Eocene rapid cooling period identified by Lossada et al. (2017) further north (30°S). Moreover, it coincides with the Eocene compressive stage widely documented north of 28°S in the Puna/Altiplano and Eastern Cordillera (Hongn et al., 2007), and it is equivalent to the Incaic orogenic phase defined by Steinmann (1929) for the northern Central Andes. This correlation implies the southward extension of the western Eocene belt defined by Lossada et al. (2017) toward the latitude of the study area (36°30′S). According to the authors, this western belt comprises the High Andes and Western Cordillera between 22°–35°S and 68°–70°W, and describes a gradual decrease of shortening from north to south. At a plate margin scale, the Eocene contractional period matches the gradual acceleration in oceanic spreading rates and plate motion after ~55-50 Ma (Colli et al., 2014; Müller et al., 2016), and the reconstructions of the subducting slab evolution that evidence coupling and significant orogenic belt built-up since ~50 ± 10 Ma in the western margin of the South American plate (Faccenna et al., 2017).

7.1.5. Significance of Cooling Ages on Oligo-Miocene Deformational Episodes

The available geological information indicates that extensional deformation linked to the genesis of the Oligocene-early Miocene Cura Mallin basin was likely localized along the volcanic arc, west from the study area (Burns et al., 2006; Spikings et al., 2008; Utgé et al., 2009). The absence of reheating signals during this time in the obtained thermal histories further support those observations. Moreover, the lack of rapid cooling for the middle Miocene compressive phase in the western flank of Domuyo volcano (Figures 2 and 3, and references therein) could indicate either that the analyzed samples were already exhumed below 40 °C (lower temperature of the PRZ for AHe) by those times, and/or that the entire area was passively transported eastwards, toward the foreland, along the gently dipping regional detachment of the ChMFTB (Figure 9a).

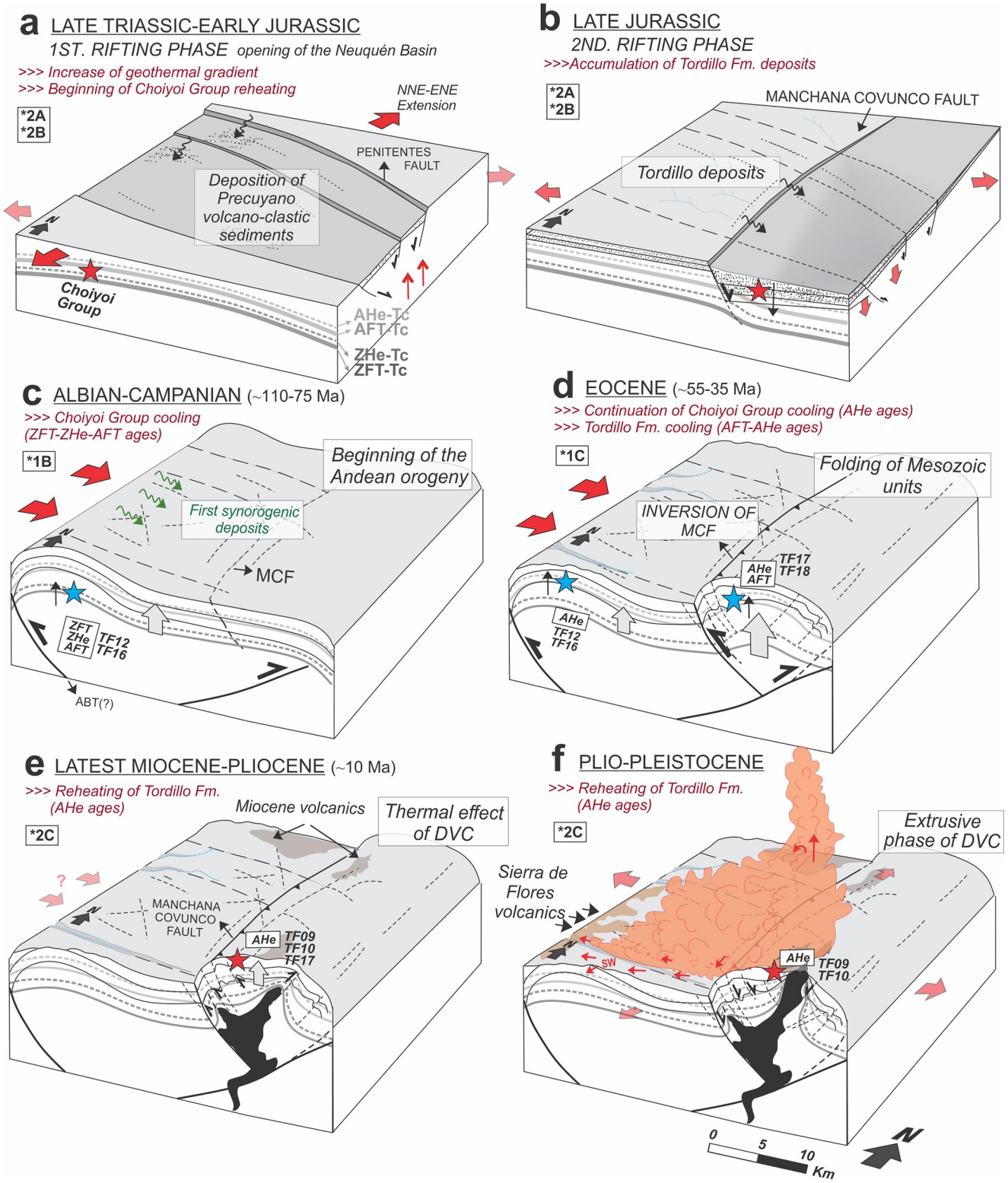

Figure 10. Schematic structural evolution of the Domuyo morpho-structure from Late Triassic to Plio-Pleistocene times. DVC: Domuyo Volcanic Complex, MCF: Manchana Covunco Fault, ABT: Andacollo back-thrust, numbers with asterisks refer to cooling/heating phases indicated in Figure 9c. See Section 7 and Galetto et al. (2018) for further details.

7.2. Mechanisms for Thrust-Related Exhumation and Implications for the Dynamics of the MCF

Contrasting thermal histories are registered on opposing sides of the MCF since Cretaceous times (Figures 8 and 9c). While Choiyoi Group samples west of the MCF remained below <100 ± 10 °C since ~80-75 Ma, the Tordillo Formation cooled below those temperatures at least 25 M.y. later. Both of these cooling periods can be explained by the inception of an east-vergent basement wedge since Late Cretaceous times combined with the development of a retro-vergent thrust to the west (Figures 9, 10c, and 10d).

As temporal variations in cooling rates depend on the amplitude of the topography, the remarkable initial steepening of the time-temperature trajectories of the Choiyoi Group samples west of the MCF requires high-angle faults capable of creating a large vertical offset associated with a rapid cooling signal (Ehlers & Farley, 2003; Metcalf et al., 2009; ter Voorde et al., 2004). In this scenario, the first rapid cooling episode of the Choiyoi Group at ~110 Ma (Figures 8a, 8b, and 9c) could be related to regional uplift in the hangingwall of an east-vergent basement wedge accommodated by a high angle and deep detachment and the inception of a retro-vergent thrust west of the Choiyoi Group units (Figures 9 and 10c). This tectonic scenario is compatible with the large basement-involved fault-bend anticline proposed for the Cordillera del Viento immediately south of the study area (Folguera et al., 2007; Kozlowski et al., 1996, 1998; Sánchez et al., 2018, 2020; Zapata et al., 1999). Moreover, displacement on a thrust fault alone does not cause exhumation; denudation is required to cool rocks and bring them to the surface (Ehlers & Farley, 2003). The active compressional deformation and the development of a broad antiform with a N-S trending axis must have enhanced the relief and triggered erosion of the Mesozoic sedimentary sequence overlying the basement and the Choiyoi Group rocks, which is reflected in a distinctive acceleration of the exhumation and cooling rates to up to 12 ± 4–23 ± 10 °C/Ma (Figures 9 and 10c; Table S4.2). The erosive products were transported and deposited eastwards in the Neuquén Group deposits, simultaneous with the development of the Cretaceous foreland basin (Di Giulio et al., 2012, 2016; Mpodozis & Ramos, 1990; Ramos, 1981; Tunik et al., 2010). As previously mentioned, the onset of rapid cooling at 110 Ma (±3 Ma considering the 95% confidence intervals for the average) is consistent with the maximum depositional ages of 109–100 Ma reported for Neuquén Group synorogenic deposits at 35°–38°S (Borghi et al., 2019; Di Giulio et al., 2012, 2016; Fennell et al., 2015; Gómez et al., 2019; Tunik et al., 2010). Therefore, erosion would have started almost simultaneously with the onset of uplift of Choiyoi Group units, with generation of positive relief and intense denudation. A humid paleoclimate has been described for Upper Cretaceous deposits at 34°–37°S (Borghi et al., 2019; Lothari et al., 2020), and climate reconstructions based on the study of contemporary foreland deposits in the Patagonian Andes indicate global greenhouse conditions for middle Cretaceous times (Varela et al., 2018, and references therein). This climate pattern supports the massive removal of the easily erodible Mesozoic sedimentary rocks overlying the basement of the Neuquén Basin, resulting in a remarkable acceleration of exhumation rates since ~110 Ma.

During the Eocene, a second compressive event controlled the local reactivation and inversion of the MCF, and the folding of the entire Mesozoic sedimentary sequence (Figures 9 and 10d). In this tectonic scenario, the MCF acted as a local retro-vergent thrust that localized most of the deformation and exhumation in the Domuyo mountain, reflected by AFT and AHe ages from the Tordillo Formation east of the MCF (Tables 1 and 2; Figure 10d). Thermal effects of the Eocene compressive stage can also be recognized in one of the Choiyoi Group thermal models (TF12), showing that the western reverse fault likely experienced some Eocene contractional reactivation, probably due to the transference of deformation through the ENE Covunco fault (Figure 5). As previously mentioned, this episode of uplift is coherent with the angular unconformity carved over Paleogene rocks of the Malargüe Group between ~36°S and 37°S (Figure 4).

The Late Cretaceous exhumation episode is not recorded by AFT cooling ages from the Tordillo Formation; this probably relates to deeper Cretaceous burial depths of this unit east of the MCF, compared to the Choiyoi Group to the west. This setting results in contrasting exhumation episodes across the AFT PRZ between the two sides of the MCF (Figure 9c). Therefore, if the MCF was a local east-dipping normal fault during the Late Jurassic, it could have controlled the distribution and thickness variations of the Upper Jurassic sedimentary rocks generating subsidence and promoting sediment accumulation in an Upper Jurassic depocenter to the east (Figure 10b) (Galetto et al., 2018). This structural architecture matches the Late Jurassic extensional tectonic configuration proposed for 34°–36°30′S in the Malargüe fold-and-thrust belt and the

Andean fore-arc during Late Jurassic times (Charrier, 2007; Charrier et al., 2007; Mescua et al., 2020; Vergara et al., 1995).

In the case of the reverse fault located west of the Choiyoi Group units, it would represent the continuation of the Andacollo back-thrust system, a Late Cretaceous, east-dipping and N-S-striking, blind back-thrust that spans the western flank of Cordillera del Viento, reaching the latitude of the Domuyo volcano (Figure 2; Cobbold & Rossello, 2003; Sánchez et al., 2018, 2020; Zapata et al., 1999).

7.3. Thermal Effects From the Emplacement of Domuyo Volcanic Complex (DVC)

The thermal impact of the intrusive phase of the DVC is constrained by the AHe cooling ages of the Tordillo Formation and reflected in the modeled thermal histories (Figures 8, 9c,, and 10f). The progressive emplacement of the DVC intrusive body and associated diffusion of heat likely controlled the latest Miocene reheating event seen in the Tordillo Formation thermal paths. The intensity and acceleration of this thermal overprint appear to be proportional to the distance of each sample from the intrusion, being more pronounced for TF10 and smoother for TF17 (Figures 5, 8d and 8e). The onset of the DVC magmatism took place during middle-late Miocene times according to its thermal effect on nearby Late Jurassic units (~10 Ma; AHe). This age is older than the 2.5 ± 0.5 Ma age suggested for the DVC by Miranda (1996), but consistent with the interpretation of middle Miocene to lower Pleistocene by Llambías et al. (1978). The extension of DVC volcanic activity toward Plio-Pleistocene times (Figure 10f) is evidenced by the protracted thermal imprint on the closest sample analyzed (TF09; Figure 5), which yielded Pleistocene AHe cooling ages (Table 2).

8. Conclusions

Inverse thermal modeling of apatite and zircon fission track and (U-Th-Sm)/He data from Paleozoic igneous rocks and Upper Jurassic sedimentary rocks from the Domuyo volcano area, reveals a stepwise thermal history composed of two major episodes of rapid cooling constrained to Albian-Campanian (~110-75 Ma) and Eocene (~55-35 Ma) times. A Paleocene quiescence stage, characterized by very slow cooling rates, separates both cooling phases (~75-55 Ma). Thermal histories from the footwall (Paleozoic samples) and hanging wall (Upper Jurassic samples) of the Manchana Covunco fault suggest differential (temporally offset) cooling trajectories. Paleozoic (Choiyoi Group) samples west of Manchana Covunco fault cooled below <100 ± 10 °C at ~80 Ma and were cooled toward the present surface since that time. The Albian onset of cooling at ~110 Ma in the structural basement units is constrained by ZFT ages from one of the analyzed samples. In turn, Upper Jurassic sedimentary samples (Tordillo Formation) east of Manchana Covunco fault cooled below the AFT PRZ at least 25 M.y. later and were subsequently affected by a late Miocene-Pleistocene reheating event. This thermal overprint is registered for those Tordillo Formation samples located closer to the main intrusive body of the Domuyo Volcanic Complex.

The constrained cooling phases likely reflect stages of exhumation driven by contractional tectonics during Albian-Campanian and Eocene times. In this context, we propose an onset of exhumation in the inner part of the Chos Malal fold-and-thrust belt for the Albian, which is ca. 25 M.y. earlier than previously constrained by low-temperature thermochronology and supported by maximum depositional ages of coeval sedimentary rocks in the foreland. Moreover, we support the idea of a continuation of the Eocene contraction widely recognized in the Puna-Eastern Cordillera and the Principal/Frontal Cordillera further south until the latitude of the study area. The recognition of contrasted cooling phases between both sides of the Manchana Covunco fault allows us to suggest that the fault was inverted during Eocene times. The positive inversion of the east-dipping normal Manchana Covunco fault as a local retro-vergent thrust has been responsible for the rapid exhumation and deformation of Tordillo Formation in its hanging wall.

The results presented here suggest that the cooling/exhumation history of Domuyo area represents a complex combination of early Andean deformational episodes with a superimposed reheating event triggered by the emplacement of the Domuyo Volcanic Complex magmatic activity since the middle-late Miocene (~10 Ma). The new data provided in this work suggest that further studies are needed to better understand the relative importance of the first mountain building stages in the Southern Andes, and their role in the structuration of the Chos Malal fold-and-thrust belt.

Data Availability Statement

All of the supplementary data have been filed at the Geochron data base (http://www.geochron.org/dataset/html/geochron_dataset_2021_05_05_GZM32).

Acknowledgments
New data used to generate the results of Tables 1 and 2, and displayed in Figures 6–10 belongs to this work and are available in the Supporting Information (S1, S2, S3, and S4). Data displayed in Figures 2 and 3 are available through Muñoz (1996), Jordan et al. (2001), Burns (2002, 2006), Cobbold and Rossello (2003), Folguera et al. (2003, 2006, 2007, 2015), García Morabito and Folguera (2005), Kay et al. (2006), Melnick et al. (2006), Burns et al. (2006), Zamora Valcarce et al. (2006, 2007, 2009), Messager et al. (2010), Tunik et al. (2010), Thomson et al. (2010), Sagripanti et al. (2011, 2012, 2015, 2016, 2017), Di Giulio et al. (2012, 2016), Cerimedo et al. (2013), Gürer et al. (2015), Rojas Vera et al. (2015), Fennell et al. (2015, 2019), and Sánchez et al. (2018, 2020). Data displayed in Figure 4 are available through JICA (1983, 1984), Llambías et al. (1978, 2007), Nullo et al. (2005), Miranda et al. (2006), Arregui et al. (2011), Orts et al. (2012), and Sagripanti et al. (2011, 2012). Data displayed in Figure 5 are available from Galetto et al. (2018). This work is based on research within A. Galetto's Ph.D. project and supported by CONICET and Fundación YPF (FYPF); subsidies from the Agencia de Promoción Científica y Tecnológica (PIO13320130100212CO, PICT-2014-2240 and PICT-2017-3259); Bec.Ar. and GeoX Research Network for Geosciences in Berlin and Potsdam. V. Georgieva's coauthorship was supported by the Chilean Government FONDECYT Postdoctoral Grant 2020 No. 3200375 and the German Science Foundation (DFG) grants to Todd Ehlers (EH329/18-1, University of Tübingen, Germany) and Manfred R. Strecker (STR&373/33B1, University of Potsdam, Germany). We appreciate the important collaboration of La.Te. Andes S.A. We would especially like to thank the Instituto de Investigación en Paleobiología y Geología and Río Negro University, Sofía Díaz Presas, Rodrigo Suárez, Andrés Gentile, and the park rangers of Domuyo Natural Protected Area who helped enormously to carry out fieldwork. We thank Dr. Ricardo Astini for his constructive review and Dr. Julie Fosdick for her insightful comments that helped to refine and clarify this manuscript.

References

Aguirre-Urreta, M. B., Tunik, M., Naipauer, M., Pazos, P., Ottone, E., Fanning, M., & Ramos, V. A. (2010). Malargüe Group (Maastrichtian-Danian) deposits in the Neuquén Andes, Argentina: Implications for the onset of the first Atlantic transgression related to Western Gondwana break-up. *Gondwana Research*, *19*(2), 482–494. https://doi.org/10.1016/j.gr.2010.06.008

Arregui, C., Carbone, O., & Leanza, H. A. (2011). Contexto tecto-sedimentario. *Congreso Geológico Argentino*, *18*, 29–36.

Astort, A., Walter, T. R., Ruiz, F., Sagripanti, L., Nacif, A., Acosta, G., & Folguera, A. (2019). Unrest at Domuyo Volcano, Argentina, detected by geophysical and geodetic data and morphometric analysis. *Remote Sensing*, *11*(18), 2175. https://doi.org/10.3390/rs11182175

Azcuy, C. L., & Caminos, R. (1987). Diastrofismo. In Archangelsky (Ed.), *El Sistema Carbonífero en la República Argentina* (pp. 239–251). Academia Nacional de Ciencias.

Balgord, E. A., & Carrapa, B. (2016). Basin evolution of upper Cretaceous-lower Cenozoic strata in the Malargüe fold-and-thrust belt: Northern Neuquén basin, Argentina. *Basin Research*, *28*(2), 183–206. https://doi.org/10.1111/bre.12106

Borghi, P., Fennell, L., Omil, R. G., Naipauer, M., Acevedo, E., & Folguera, A. (2019). The Neuquén group: The reconstruction of a late Cretaceous foreland basin in the southern Central Andes (35-37°S). *Tectonophysics*, *767*, 228177. https://doi.org/10.1016/j.tecto.2019.228177

Brandon, M. T., Roden-Tice, M. K., & Garver, J. I. (1998). Late Cenozoic exhumation of the Cascadia accretionary wedge in the Olympic mountains, Northwest Washington State. *Geological Society of America Bulletin*, *110*(8), 985B1009. https://doi.org/10.1130/0016-7606(1998)110<0985:lceotc>2.3.co;2

Burns, W. M. (2002). *Tectonic and depositional evolution of the Tertiary Cura Mallín basin in the southern Andes (36.5° to 38°SL) (Ph.D. Thesis, p. 218). Cornell University*.

Burns, W. M., Jordan, T. E., Copeland, P., & Kelley, S. A. (2006). The case for extensional tectonics in the Oligocene-Miocene Southern Andes as recorded in the Cura Mallin basin (36°-38°S). *Special Papers-Geological Society of America*, *407*, 163. https://doi.org/10.1130/2006.2407(08

Burtner, R. L., Nigrini, A., & Donelick, R. A. (1994). Thermochronology of lower Cretaceous source rocks in the Idaho-Wyoming thrust belt. *The American Association of Petroleum Geologists Bulletin*, *78*, 1613–1636.

Carbone, O., Franzese, J., Limeres, M., Delpino, D., & Martínez, R. (2011). *El Ciclo Precuyano (Triásico tardío-Jurásico temprano) en la Cuenca Neuquina* (pp. 63–76). Relatorio Geología y Recursos Naturales de la provincia del Neuquén.

Casé, A. M., López-Escobar, L., Danieli, J. C., & Schalamuk, A. (2008). Butalón igneous rocks, Neuquén, Argentina: Age, stratigraphic relationships and geochemical features. *Journal of South American Earth Sciences*, *26*, 188–203. https://doi.org/10.1016/j.jsames.2007.11.001

Cerimedo Álvarez, J., Orts, D., Rojas Vera, E., Folguera, A., Bottesi, G., & Ramos, V. A. (2013). Mecanismos y fases de construcción orogénicos del frente oriental andino (36°S, Argentina). *Andean Geology*, *40*(3), 504–520.

Charrier, R. (2007). Kimmeridgian back-arc extensional reactivation and magmatism in the northern and central Chilean Andes (21°–36° LS). In *Abstracts of Geosur 2007* (pp. 22–25).

Charrier, R., Pinto, L., & Rodríguez, M. P. (2007). Tectono-stratigraphic evolution of the Andean orogen in chile. In T. Moreno & W. Gibbons (Eds.), *En the Geology of Chile* (pp. 21–114). The Geological Society.

Chiodini, G., Liccioli, C., Vaselli, O., Calabrese, S., Tassi, F., Caliro, S., et al. (2014). The Domuyo volcanic system: An enormous geothermal resource in Argentine Patagonia. *Journal of Volcanology and Geothermal Research*, *274*, 71–77. https://doi.org/10.1016/j.jvolgeores.2014.02.006

Cobbold, P. R., Diraison, M., & Rossello, E. A. (1999). Bitumen veins and Eocene transpression, Neuquén Basin, Argentina. *Tectonophysics*, *314*, 423–442. https://doi.org/10.1016/s0040-1951(99)00222-x

Cobbold, P. R., & Rossello, E. A. (2003). Aptian to recent compressional deformation, foothills of the Neuquén Basin, Argentina. *Marine and Petroleum Geology*, *20*, 429–443. https://doi.org/10.1016/S0264-8172(03)00077-1

Colavitto, B., Sagripanti, L., Fennell, L., Folguera, A., & Costa, C. (2019). Evidence of quaternary tectonics along Río Grande valley, southern Malargüe fold and thrust belt, Mendoza, Argentina. *Geomorphology*, *346*, 106812. https://doi.org/10.1016/j.geomorph.2019.06.025

Colavitto, B., Sagripanti, L., Jagoe, L., Costa, C., & Folguera, A. (2020). Quaternary tectonics in the southern Central Andes (37º-38°S): Retroarc compression inferred from morphotectonics and numerical models. *Journal of South American Earth Sciences*, *102*, 102697.

Colli, L., Stotz, I., Bunge, H. P., Smethurst, M., Clark, S., Iaffaldano, G., et al. (2014). Rapid South Atlantic spreading changes and coeval vertical motion in surrounding continents: Evidence for temporal changes of pressure-driven upper mantle flow. *Tectonics*, *33*. 1304–1321. https://doi.org/10.3997/2214-4609.20141654

Di Giulio, A., Ronchi, A., Sanfilippo, A., Balgord, E. A., Carrapa, B., & Ramos, V. A. (2016). Cretaceous evolution of the Andean margin between 36°S and 40°S latitude through a multi-proxy provenance analysis of Neuquén Basin strata (Argentina). *Basin Research*, *29*(3), 284–304. https://doi.org/10.1111/bre.12176

Di Giulio, A., Ronchi, A., Sanfilippo, A., Tiepolo, M., Pimentel, M., & Ramos, V. A. (2012). Detrital zircon provenance from the Neuquén Basin (south-central Andes): Cretaceous geodynamic evolution and sedimentary response in a retroarc-foreland basin. *Geology*, *40*(6), 559–562. https://doi.org/10.1130/G33052.1

Dodson, M. H. (1973). Closure temperature in cooling geochronological and petrological systems. *Contributions to Mineralogy and Petrology*, *40*, 259–274. https://doi.org/10.1007/BF00373790

Donelick, R. A. (1993). A method of fission track analysis utilizing bulk chemical etching of apatite. *U.S. Patent*, *5*, 267–274.

Dunkl, I. (2002). TRACKKEY: A windows program for calculation and graphical presentation of fission track data. *Computers and Geosciences*, *28*(1), 3–12. https://doi.org/10.1016/s0098-3004(01)00024-3

Echaurren, A., Folguera, A., Gianni, G., Orts, D., Tassara, A., Encinas, A., et al. (2016). Tectonic evolution of the North Patagonian Andes (41°-44° S) through recognition of syntectonic strata. *Tectonophysics*, *677–678*, 99–114. https://doi.org/10.1016/j.tecto.2016.04.009

Ehlers, T. A., & Farley, K. A. (2003). Apatite (U–Th)/He thermochronometry: Methods and applications to problems in tectonic and surface processes. *Earth and Planetary Science Letters*, *206*(1–2), 1–14. https://doi.org/10.1016/s0012-821x(02)01069-5

Faccenna, C., Oncken, O., Holt, A. F., & Becker, T. W. (2017). Initiation of the Andean orogeny by lower mantle subduction. *Earth and Planetary Science Letters*, *463*, 189–201. https://doi.org/10.1016/j.epsl.2017.01.041

Farley, K. A. (2000). Helium diffusion from apatite: General behavior as illustrated by Durango fluorapatite. *Journal of Geophysical Research*, *105*, 2903–2914. https://doi.org/10.1029/1999JB900348

Farley, K. A. (2002). (U-Th)/He dating: Techniques, calibrations, and applications. *Reviews in Mineralogy and Geochemistry*, *47*(1), 819–844. https://doi.org/10.2138/rmg.2002.47.18

Farley, K. A., Wolf, R. A., & Silver, L. T. (1996). The effects of long alpha-stopping distances on (U-Th)/He ages. *Geochimica et Cosmochimica Acta*, *60*(21), 4223–4229. https://doi.org/10.1016/s0016-7037(96)00193-7

Fennell, L. M., Folguera, A., Naipauer, M., Gianni, G., Rojas Vera, E., Bottesi, G., & Ramos, V. A. (2015). Cretaceous deformation of the southern Central Andes: Synorogenic growth strata in the Neuquén Group (35°30′–37°SL). *Basin Research*, *29*(3), 1–22. https://doi.org/10.1111/bre.12135

Fennell, L. M., Iannelli, S. B., Encinas, A., Naipauer, M., Valencia, V., & Folguera, A. (2019). Alternating contraction and extension in the Southern Central Andes (35°-37°S). *American Journal of Science*, *319*, 381–429. https://doi.org/10.2475/05.2019.02

Fleischer, R. L., Price, P. B., & Walker, R. M. (1975). *Nuclear tracks in solids: Principles and applications*. University of California Press. https://doi.org/10.1525/9780520320239

Flowers, R. M., & Farley, K. A. (2012). Apatite ^{4}He/^{3}He and (U-Th)/He evidence for an Ancient Grand Canyon. *Science*, *338*, 1616–1619. https://doi.org/10.1126/science.1229390

Flowers, R. M., & Farley, K. A. (2013). Response to comments on "Apatite ^{4}He/^{3}He and (U-Th)/He evidence for an Ancient Grand Canyon". *Science*, *340*(6129), 143. https://doi.org/10.1126/science.1234203

Flowers, R. M., Ketcham, R. A., Shuster, D. L., & Farley, K. A. (2009). Apatite (U-Th)/He thermochronometry using a radiation damage accumulation and annealing model. *Geochimica et Cosmochimica Acta*, *73*(8), 2347–2365. https://doi.org/10.1016/j.gca.2009.01.015

Folguera, A., Bottesi, G., Duddy, I., Martín-González, F., Orts, D., Sagripanti, L., et al. (2015). Exhumation of the Neuquén Basin in the southern Central Andes (Malargüe fold and thrust belt) from field data and low-temperature thermochronology. *Journal of South American Earth Sciences*, *64*, 381–398. https://doi.org/10.1016/j.jsames.2015.08.003

Folguera, A., Ramos, V. A., & Melnick, D. (2003). Recurrencia en el desarrollo de cuencas de intra-arco, Cordillera Neuquina (37° 30′-38°S). *Revista de la Asociación Geológica Argentina*, *58*(1), 3–19.

Folguera, A., Ramos, V. A., Zapata, T. R., Spagnuolo, M., & Miranda, F. (2005). Pliocene to Quaternary retro-arc extension in the Andes at 35°-37°30'SL. *In 6th International Symposium on Andean Geodynamics* (pp. 277–280). Extended Abstracts.

Folguera, A., Ramos, V. A., Zapata, T., & Spagnuolo, M. G. (2007). Andean evolution at the Guañacos and Chos Malal fold and thrust belts (36°30′-37°S). *Journal of Geodynamics*, *44*, 129–148. https://doi.org/10.1016/j.jog.2007.02.003

Folguera, A., Zapata, T., & Ramos, V. A. (2006). Late Cenozoic extension and the evolution of the Neuquén Andes. *Special Papers-Geological Society of America*, *407*, 267.

Fosdick, J. C., Romans, B. W., Fildani, A., Bernhardt, A., Calderon, M., & Graham, S. A. (2011). Kinematic evolution of the Patagonian retroarc fold-and-thrust belt and Magallanes foreland basin, Chile and Argentina, 51°30'S. *Geological Society of America Bulletin*, *123*, 1679–1698. https://doi.org/10.1130/b30242.1

Franchini, M., López-Escobar, L., Schalamuk, I. B. A., & Meinert, L. (2003). Magmatic characteristics of the paleocene cerro nevazón region and other late Cretaceous to early tertiary calc-alkaline subvolcanic to plutonic units in the Neuquén Andes, Argentina. *Journal of South American Earth Sciences*, *16*, 399–421. https://doi.org/10.1016/S0895-9811(03)00103-2

Franzese, J. R., & Spalletti, L. A. (2001). Late Triassic-early Jurassic continental extension in southwestern Gondwana: Tectonic segmentation and pre-break-up rifting. *Journal of South American Earth Sciences*, *14*, 257–270. https://doi.org/10.1016/S0895-9811(01)00029-3

Franzese, J., Spalletti, L., Pérez, I. G., & Macdonald, D. (2003). Tectonic and paleoenvironmental evolution of mesozoic sedimentary basins along the Andean foothills of Argentina (32°-54°S). *Journal of South American Earth Sciences*, *16*, 81–90. https://doi.org/10.1016/s0895-9811(03)00020-8

Fuentes, F., & Horton, B. K. (2020). The Andean foreland evolution of the Neuquén basin: A discussion. In *Opening and closure of the Neuquén Basin in the southern Andes* (pp. 341–370). Springer. https://doi.org/10.1007/978-3-030-29680-3_14

Galbraith, R. F. (1981). On statistical models for fission track counts. *Mathematical Geology*, *13*(6), 471–478. https://doi.org/10.1007/bf01034498

Galetto, A., García, V., & Caselli, A. (2018). Structural controls of the Domuyo geothermal field, Southern Andes (36°38′S), Argentina. *Journal of Structural Geology*, *114*, 76–94. https://doi.org/10.1016/j.jsg.2018.06.002

Gallagher, K. (2012). Transdimensional inverse thermal history modeling for quantitative thermochronology. *Journal of Geophysical Research*, *117*, B02408. https://doi.org/10.1029/2011JB008825

Gallagher, K., Charvin, K., Nielsen, S., Sambridge, M., & Stephenson, J. (2009). Markov chain Monte Carlo (MCMC) sampling methods to determine optimal models, model resolution and model choice for Earth Science problems. *Marine and Petroleum Geology*, *26*, 525–535. https://doi.org/10.1016/j.marpetgeo.2009.01.003

Gallagher, K., & Ketcham, R. A. (2020). Comment on the reply to the Comment on "Thermal history modelling: HeFTy vs. QTQt" by Vermeesch and Tian, Earth-Science Reviews (2014). *Earth-Science Reviews*, *139*, 279–290.

Galland, O., Hallot, E., Cobbold, P. R., Ruffet, G., & de Bremond d'Ars, J. (2007). Volcanism in a compressional Andean setting: A structural and geochronological study of Tromen volcano (Neuquén province, Argentina). *Tectonics*, *26*, TC4010. https://doi.org/10.1029/2006TC002011

García Morabito, E., & Folguera, A. (2005). El alto de Copahue-Pino Achado y la fosa de Loncopué: Un comportamiento tectónico episódico, Andes neuquinos (37°-39°S). *Revista de Asociación Geológica Argentina*, *60*(40), 742–761.

Gehrels, G. E., Valencia, V. A., & Ruiz, J. (2008). Enhanced precision, accuracy, efficiency, and spatial resolution of U-Pb ages by laser ablation-multicollector-inductively coupled plasma-mass spectrometry. *Geochemistry, Geophysics, Geosystems*, *9*, Q03017. https://doi.org/10.1029/2007GC001805

Genge, M. C., Zattin, M., Savignano, E., Franchini, M., Gautheron, C., Ramos, V. A., & Mazzoli, S. (2021). The role of slab geometry in the exhumation of cordilleran-type orogens and their forelands: Insights from northern Patagonia. *Geological Society of America Bulletin*. https://doi.org/10.1130/b35767.1

Georgieva, V., Melnick, D., Schildgen, T. F., Ehlers, T. A., Lagabrielle, Y., Enkelmann, E., & Strecker, M. R. (2016). Tectonic control on rock uplift, exhumation, and topography above an oceanic ridge collision: Southern Patagonian Andes (47°S), Chile. *Tectonics*, *35*, 1317–1341. https://doi.org/10.1002/2016TC004120

Ghiglione, M. C., Likerman, J., Barberón, V., Beatriz Giambiagi, L., Aguirre-Urreta, B., & Suarez, F. (2014). Geodynamic context for the deposition of coarse-grained deep-water axial channel systems in the Patagonian Andes. *Basin Research*, *26*(6), 726–745. https://doi.org/10.1111/bre.12061

Giacosa, R., Allard, J., Foix, N., & Heredia, N. (2014). Stratigraphy, structure and geodynamic evolution of the Paleozoic rocks in the Cordillera del Viento (37°SL, Andes of Neuquén, Argentina). *Journal of Iberian Geology*, *40*(2), 331–348. https://doi.org/10.5209/rev_jige.2014.v40.n2.45301

Gianni, G. M., Dávila, F. M., Echaurren, A., Fennell, L., Tobal, J., Navarrete, C., et al. (2018). A geodynamic model linking Cretaceous orogeny, arc migration, foreland dynamic subsidence and marine ingression in southern South America. *Earth-Science Reviews*, *185*, 437–462. https://doi.org/10.1016/j.earscirev.2018.06.016

Gleadow, A. J. W., & Fitzgerald, P. G. (1987). Uplift history and structure of the transantarctic mountains: New evidence from fission track dating of basement apatites in the Dry Valleys area, southern Victoria Land. *Earth and Planetary Science Letters*, *82*, 1–14. https://doi.org/10.1016/0012-821x(87)90102-6

Glodny, J., Gräfe, K., Echtler, H., & Rosenau, M. (2008). Mesozoic to quaternary continental margin dynamics in South-Central Chile (36°-42°S): The apatite and zircon fission track perspective. *International Journal of Earth Sciences*, *97*(6), 1271–1291. https://doi.org/10.1007/s00531-007-0203-1

Gómez, R., Lothari, L., Tunik, M., & Casadio, S. (2019). Onset of foreland basin deposition in the Neuquén Basin (34°-35°S): New data from sedimentary petrology and U-Pb dating of detrital zircons from the Upper Cretaceous non-marine deposits. *Journal of South American Earth Sciences*, *95*, 102257. https://doi.org/10.1016/j.jsames.2019.102257

Green, P. F. (1981). A new look at statistics in fission track dating. *Nuclear Tracks and Radiation Measurements*, *5*(1–2), 77–86. https://doi.org/10.1016/0191-278X(81)90029-9

Green, P. F., Duddy, I. R., Gleadow, A. J. W., Tingate, P. R., & Laslett, G. M. (1986). Thermal annealing of fission tracks in apatite. *Chemical Geology: Isotope Geoscience section*, *59*, 237–253. https://doi.org/10.1016/0168-9622(86)90074-6

Guenthner, W. R., Reiners, P. W., Ketcham, R. A., Nasdala, L., & Giester, G. (2013). Helium diffusion in natural zircon: Radiation damage, anisotropy, and the interpretation of zircon (U-Th)/He thermochronology. *American Journal of Science*, *313*(3), 145–198. https://doi.org/10.2475/03.2013.01

Gürer, D., Galland, O., Corfu, F., Leanza, H. A., & Sassier, C. (2015). Structure and evolution of volcanic plumbing systems in fold-and-thrust belts: A case study of the Cerro Negro de Tricao Malal, Neuquén Province, Argentina. *Geological Society of America Bulletin*, *128*(1–2), 315–331. https://doi.org/10.1130/B31341.1

Hongn, F., Papa, C. D., Powell, J., Petrinovic, I., Mon, R., & Deraco, V. (2007). Middle Eocene deformation and sedimentation in the Puna-Eastern Cordillera transition (23°-26°S): Control by preexisting heterogeneities on the pattern of initial Andean shortening. *Geology*, *35*(3), 271–274. https://doi.org/10.1130/g23189a.1

Horton, B. K. (2018). Tectonic regimes of the central and southern Andes: Responses to variations in plate coupling during subduction. *Tectonics*, *37*, 402–429. https://doi.org/10.1002/2017TC004624

Hurford, A. J. (1986). Cooling and uplift patterns in the Lepontine Alps South Central Switzerland and an age of vertical movement on the insubric fault line. *Contributions to Mineralogy and Petrology*, *92*, 413–427. https://doi.org/10.1007/BF00374424

Hurford, A. J., & Green, P. F. (1983). The zeta age calibration of fission-track dating. *Chemical Geology*, *41*, 285–317. https://doi.org/10.1016/s0009-2541(83)80026-6

Iannelli, S. B., Fennell, L., Fernández Paz, L., Litvak, V. D., Encinas, A., & Folguera, A. (2020). Late Cretaceous to Oligocene magmatic evolution of the Neuquén basin. In *Opening and closure of the Neuquén Basin in the southern Andes* (pp. 397–416). Springer. https://doi.org/10.1007/978-3-030-29680-3_16

JICA. (1983). *Interim report on the northern Neuquén geothermal development project. First-second phase survey* (unpublished, p. 85). Japan International Cooperation Agency-Ente Provincial de Energía de la Provincia de Neuquén. Retrieved from https://openjicareport.jica.go.jp/643/643/643_701_10299998.html

JICA. (1984). *Final report on the northern Neuquén geothermal development project. Third phase survey* (unpublished, p. 105). Japan International Cooperation Agency-Ente Provincial de Energía de la Provincia de Neuquén. Retrieved from https://openjicareport.jica.go.jp/643/643/643_701_10299998.html

Jordan, T. E., Burns, W. M., Veiga, R., Pángaro, F., Copeland, P., Kelley, S., & Mpodozis, C. (2001). Extension and basin formation in the Southern Andes caused by increased convergence rate: A Mid-Cenozoic trigger for the Andes. *Tectonics*, *20*, 308–324. https://doi.org/10.1029/1999TC001181

Kay, S. M., Burns, W. M., Copeland, P., & Mancilla, O. (2006). Upper Cretaceous to Holocene magmatism and evidence for transient Miocene shallowing of the Andean subduction zone under the northern Neuquén Basin. *Geological Society of America*, *407*, 19.

Kelley, S. A. (2005). Low-temperature cooling histories of the Cheyenne belt and Laramie peak shear zone, Wyoming, and the soda creek-fish creek shear zone, Colorado. In K. E. Karlstrom & G. R. Keller (Eds.), *The Rocky mountain region: An evolving lithosphere* (Vol. 154, pp. 55–70). American Geophysical Union, Geophysical Monograph Series. https://doi.org/10.1029/154GM05

Ketcham, R. A., Carter, A., Donelick, R. A., Barbarand, J., & Hurford, A. J. (2007). Improved modeling of fission-track annealing in apatite. *American Mineralogist*, *92*(5–6), 799–810. https://doi.org/10.2138/am.2007.2281

Ketcham, R. A., Donelick, R. A., & Carlson, W. D. (1999). Variability of apatite fission-track annealing kinetics; III. Extrapolation to geological time scales. *American Mineralogist*, *84* (9), 1235–1255. https://doi.org/10.2138/am-1999-0903

Klepeis, K., Betka, P., Clarke, G., Fanning, M., Hervé, F., Rojas, L., et al. (2010). Continental underthrusting and obduction during the Cretaceous closure of the Rocas Verdes rift basin, Cordillera Darwin, Patagonian Andes. *Tectonics*, *29*, TC3014. https://doi.org/10.1029/2009TC002610

Kozlowski, E., Cruz, C., & Rebay, G. (1987). El Terciario volcaniclástico de la zona Puntilla del Huincan. Mendoza. In *Congreso Geológico Argentino, No. 10, Actas* (Vol. 4, pp. 229–232).

Kozlowski, E. E., Cruz, C. E., & Sylwan, C. A. (1996). Geología estructural de la zona de Chos Malal, Cuenca Neuquina, Argentina. *Relatorio del XIII Congreso Geológico Argentino y III Congreso de Exploración de Hidrocarburos*, *1*, 15–26.

Kozlowski, E. E., Cruz, C. E., & Sylwan, C. A. (1998). Modelo exploratorio en la faja corrida de la Cuenca Neuquina, Argentina. *Bol Inf Petrol*, *55*, 4–23.

Laslett, G. M., Green, P. F., Duddy, I. R., & Gleadow, A. J. W. (1987). Thermal annealing of fission tracks in apatite 2. A quantitative analysis. *Chemical Geology: Isotope Geoscience section*, *65*, 1–13. https://doi.org/10.1016/0168-9622(87)90057-1

Leanza, H. A., & Hugo, C. A. (2001). Cretaceous red beds from southern Neuquén Basin (Argentina): Age, distribution and stratigraphic discontinuities. *Publicación Electrónica de la Asociación Paleontológica Argentina*, *7*(1).

Legarreta, L., & Uliana, M. A. (1999). El Jurásico y Cretácico de la Cordillera Principal y la cuenca Neuquina. 1. Facies sedimentarias. In R. Caminos (Ed.), *Geología Argentina* (Vol. 29(16), pp. 399–416). Servicio Geológico y Minero Argentino, Instituto de Geología y Recursos Minerales, Anales.

Llambías, E. J., & Aragón, E. (2011). *Volcanismo Paleógeno. Geología y recursos naturales de la Provincia del Neuquén* (pp. 265–274).

Llambías, E. J., Leanza, H. A., & Carbone, O. (2007). Evolución tectono-magmática durante el Pérmico al Jurásico Temprano en la cordillera del Viento (37°05' S-37°15'S): Nuevas evidencias geológicas y geoquímicas del inicio de la Cuenca Neuquina. *Revista de la Asociación Geológica Argentina*, *62*(2), 217–235.

Llambías, E. J., Palacios, M., Danderfer, J. C., & Brogioni, N. (1978). *Petrología de las rocas ígneas cenozoicas del Volcán Domuyo y áreas adyacentes* (Vol. 2, pp. 553–584). Provincia del Neuquén, en los relatorios del 7mo Congreso Geológico Argentino.

Llambías, E. J., & Sato, A. M. (2011). *Ciclo Gondwánico: La provincia magmática Choiyoi en Neuquén* (pp. 53–62). Relatorio Geología y Recursos Naturales de la provincia del Neuquén.

Lossada, A. C., Giambiagi, L., Hoke, G. D., Fitzgerald, P. G., Creixell, C., Murillo, I., et al. (2017). Thermochronologic evidence for late Eocene Andean mountain building at 30°S. *Tectonics*, *36*, 2693–2713. https://doi.org/10.1002/2017TC004674

Lothari, L. D., Gómez, R. E., Tunik, M. A., & Casadio, S. A. (2020). Análisis de facies y petrografía de los depósitos del Cretácico superior en el norte de la Cuenca Neuquina: Implicancias para el inicio de la etapa de Foreland. *Latin American Journal of Sedimentology and Basin Analysis*, *27*(1), 3–28.

Müller, R. D., Seton, M., Zahirovic, S., Williams, S. E., Matthews, K. J., Wright, N. M., et al. (2016). Ocean basin evolution and global-scale plate reorganization events since Pangea breakup. *Annual Review of Earth and Planetary Sciences*, *44*, 107–138. https://doi.org/10.1146/annurev-earth-060115-012211

Maloney, K. T., Clarke, G. L., Klepeis, K. A., & Quevedo, L. (2013). The late Jurassic to present evolution of the Andean margin: Drivers and the geological record. *Tectonics*, *32*, 1049–1065. https://doi.org/10.1002/tect.20067

Matthews, K. J., Seton, M., & Müller, R. D. (2012). A global-scale plate reorganization event at 105–100Ma. *Earth and Planetary Science Letters*, *355–356*, 283–298. https://doi.org/10.1016/j.epsl.2012.08.023

Melnick, D., Rosenau, M., Folguera, A., & Echtler, H. (2006). Neogene tectonic evolution of the Neuquen Andes western flank (37-39°S). *Special Papers-Geological Society of America*, *407*, 73. https://doi.org/10.1130/2006.2407(04

Mescua, J. F., Giambiagi, L. B., & Ramos, V. A. (2013). Late Cretaceous uplift in the Malargüe fold-and-thrust belt (35 S), southern Central Andes of Argentina and Chile. *Andean Geology*, *40*(1), 102–116. https://doi.org/10.5027/andgeov40n1-a05

Mescua, J. F., Suriano, J., Schencman, L. J., Giambiagi, L. B., Sruoga, P., Balgord, E., & Bechis, F. (2020). Controls on deposition of the Tordillo formation in southern Mendoza (34°-36° S): Implications for the Kimmeridgian tectonic setting of the Neuquén basin. In *Opening and closure of the Neuquén Basin in the southern Andes* (pp. 127–157). Springer. https://doi.org/10.1007/978-3-030-29680-3_6

Messager, G., Nivière, B., Martinod, J., Lacan, P., & Xavier, J.-P. (2010). Geomorphic evidence for Plio-Quaternary compression in the Andean foothills of the southern Neuquén Basin, Argentina. *Tectonics*, *29*, TC4003. https://doi.org/10.1029/2009TC002609

Metcalf, J. R., Fitzgerald, P. G., Baldwin, S. L., & Muñoz, J. A. (2009). Thermochronology of a convergent orogen: Constraints on the timing of thrust faulting and subsequent exhumation of the Maladeta Pluton in the Central Pyrenean Axial Zone. *Earth and Planetary Science Letters*, *287*(3–4), 488–503. https://doi.org/10.1016/j.epsl.2009.08.036

Miranda, F. J. (1996). *Caracterización petrográfica y geoquímica del Cerro Domuyo. Pcia. de Neuquén, Argentina (Licenciatura thesis): Buenos Aires*. Facultad de Ciencias Exactas y Naturales, Universidad de Buenos Aires.

Miranda, F. J., Folguera, A., Leal, P., Naranjo, J., & Pesce, A. (2006). Upper Pliocene to lower Pleistocene volcanic complexes and upper Neogene deformation in the south-central Andes (36°30'-38°00'SL). In S. M. Kay & V. A. Ramos (Eds.), *Evolution of an Andean margin: A tectonic and magmatic view from the Andes to the Neuquén Basin (35°-39°SL)* (Vol. 407, pp. 287–298). Geological Society of America Special Paper. https://doi.org/10.1130/2006.2407(13)

Molnar, P., & Atwater, T. (1978). Interarc spreading and cordilleran tectonics as alternates related to the age of subducted oceanic lithosphere. *Earth and Planetary Science Letters*, *41*(3), 330–340. https://doi.org/10.1016/0012-821x(78)90187-5

Moore, M. A., & England, P. C. (2001). On the inference of denudation rates from cooling ages of minerals. *Earth and Planetary Science Letters*, *185*, 265–284. https://doi.org/10.1016/s0012-821x(00)00380-0

Mpodozis, C., & Ramos, V. A. (1990). The Andes of Argentina and chile. En geology of the Andes and its relation to hydrocarbon and mineral resources. In G. E. Ericksen, M. T. Cañas Pinochet, & J. A. Reinemund (Eds.), *Circumpacific Council for Energy and mineral Resources, Earth Science Series* (Vol. 11, pp. 59–90).

Muñoz, N. (1996). The thermal evolution of Jurassic and Cretaceous source rocks in the Malargüe thrust belt, Argentina: Implications for hydrocarbon exploration. In *Independent project report. Unpublished MSc course in basin evolution and dynamics* (p. 98). Department of Geology, Royal Holloway University of London.

Naipauer, M., García Morabito, E., Marques, J. C., Tunik, M., Rojas Vera, E. A., Vujovich, G. I., et al. (2012). Intraplate late Jurassic deformation and exhumation in western central Argentina: Constraints from surface data and U-Pb detrital zircon ages. *Tectonophysics*, *524–525*, 59–75. https://doi.org/10.1016/j.tecto.2011.12.017

Naipauer, M., Tapia, F., Mescua, J., Farías, M., Pimentel, M. M., & Ramos, V. A. (2015a). Detrital and volcanic zircon U-Pb ages from southern Mendoza (Argentina): An insight on the source regions in the northern part of the Neuquén Basin. *Journal of South American Earth Sciences*, *64*(2), 434–451. https://doi.org/10.1016/j.jsames.2015.09.013

Naipauer, M., Tunik, M., Marques, J. C., Rojas Vera, E. A., Vujovich, G. I., Pimentel, M. M., & Ramos, V. A. (2015b). U-Pb detrital zircon ages of Upper Jurassic continental successions: Implications for the provenance and absolute age of the Jurassic-Cretaceous boundary in the Neuquén Basin. *Geological Society, London, Special Publications*, *399*(1), 131–154. https://doi.org/10.1144/sp399.1

Norris, A., & Danyushevsky, L. (2018). *Towards estimating the complete uncertainty budget of quantified results measured by LA-ICP-MS*. Goldschmidt.

Nullo, F. E., Stephens, G., Combina, A., Dimieri, L., Baldauf, P., Bouza, P., et al. (2005). *Hoja Geológica 3569-III/3572-IV Malargüe*.

Orts, D. L., Folguera, A., Giménez, M., & Ramos, V. A. (2012). Variable structural controls through time in the Southern Central Andes (~36°S). *Andean Geology*, *39*(2), 220–241. https://doi.org/10.5027/andgeov39n2-a02

Pesce, A. H. (1987). Evaluación geotérmica del área cerro domuyo: Síntesis estratigráfica, vulcanológica, estructural y geoquímica modelo geotérmico preliminar, provincia del Neuquén, República Argentina. *In: Proceedings International Meeting on Geothermics and Geothermal Energy, Sao Paulo, Brazil, Revista Brasileira de Geofisica* (Vol. 5, pp. 283–299).

Price, P. B., & Walker, R. M. (1963). Fossil tracks of charged particles in mica and the age of minerals. *Journal of Geophysical Research*, *68*, 4847–4862. https://doi.org/10.1029/JZ068i016p04847

Ramos, V. A. (1981). Descripción geológica de la Hoja 33 c los chihuidos norte, provincia del Neuquén. *Boletin Servicio Geologico Nacional*, *182*, 1–103.

Ramos, V. A. (2009). Anatomy and global context of the Andes: Main geologic features and the Andean orogenic cycle. *Backbone of the Americas: Shallow Subduction, Plateau Uplift, and Ridge and Terrane Collision*, *204*, 31–65.

Ramos, V. A., & Folguera, A. (2009). Andean flat-slab subduction through time. *Geological Society, London, Special Publications*, *327*(1), 31–54. https://doi.org/10.1144/GSL.SP.2005.252.01.02

Ramos, V. A., & Kay, S. M. (2006). Overview of the tectonic evolution of the southern central Andes of Mendoza and Neuquén (35°-39°SL). In S. M. Kay, & V. A. Ramos (Eds.), *Evolution of the Andean margin: A tectonic and magmatic view from the Andes to the Neuquén Basin (35°-39°SL)* (Vol. 407, pp. 1–17). Geological Society of America, Special Paper.

Reiners, P. W., & Brandon, M. T. (2006). Using thermochronology to understand orogenic erosion. *Annual Review of Earth and Planetary Sciences*, *34*, 419–466. https://doi.org/10.1146/annurev.earth.34.031405.125202

Reiners, P. W., Spell, T. L., Nicolescu, S., & Zanetti, K. A. (2004). Zircon (U-Th)/He thermochronometry: He diffusion and comparisons with 40Ar/39Ar dating. *Geochimica et Cosmochimica Acta*, *68*(8), 1857–1887. https://doi.org/10.1016/j.gca.2003.10.021

Rodríguez, M. F., Leanza, H. A., Arregui, C., Carbone, O., Danieli, J. C., & Vallés, J. (2011). El grupo malargüe (cretácico tardío-paleógeno temprano) en la cuenca neuquina. In *Relatorio del 18 Congreso Geológico Argentino* (pp. 245–264).

Rojas Vera, E. A., Folguera, A., Zamora Valcarce, G., Bottesi, G., & Ramos, V. A. (2014a). Structure and development of the Andean system between 36° and 39°S. *Journal of Geodynamics*, *73*, 34–52. https://doi.org/10.1016/j.jog.2013.09.001

Rojas Vera, E. A., Mescua, J., Folguera, A., Becker, T. P., Sagripanti, L., Fennell, L., et al. (2015). Evolution of the Chos Malal and Agrio fold and thrust belts, Andes of Neuquén: Insights from structural analysis and apatite fission track dating. *Journal of South American Earth Sciences*, *64*, 418–433. https://doi.org/10.1016/j.jsames.2015.10.001

Rojas Vera, E. A., Sellés, D., Folguera, A., Gímenez, M., Ruíz, F., Orts, D., et al. (2014b). The origin of the Loncopué trough in the retro-arc of the southern central Andes from field, geophysical and geochemical data. *Tectonophysics*, *637*, 1–19. https://doi.org/10.1016/j.tecto.2014.09.012

Rossel, R., Oliveros, V., & Mescua, J. (2014). The upper Jurassic volcanism of the Río Damas-Tordillo Formation (33–35.5 S): Insights on petrogenesis, chronology, provenance and tectonic implications. *Andean Geology*, *41*(3), 529–557.

Sagripanti, L., Bottesi, G., Kietzmann, D., Folguera, A., & Ramos, V. A. (2012). Mountain building processes at the orogenic front. A study of the unroofing in Neogene foreland sequence (37°S). *Andean Geology*, *39*, 201–219. https://doi.org/10.5027/andgeov39n2-a01

Sagripanti, L., Bottesi, G., Naipauer, M., Folguera, A., & Ramos, V. A. (2011). U/Pb ages on detrital zircons in the southern central Andes Neogene foreland (36°-37°S): Constraints on Andean exhumation. *Journal of South American Earth Sciences*, *32*, 555–566. https://doi.org/10.1016/j.jsames.2011.03.010

Sagripanti, L., Colavitto, B., Jagoe, L., Andrés, F., & Costa, C. (2018). A review about the quaternary upper-plate deformation in the southern central Andes (36°-38°S): A plausible interaction between mantle dynamics and tectonics. *Journal of South American Earth Sciences*, *87*, 221–231. https://doi.org/10.1016/j.jsames.2017.11.008

Sagripanti, L., Folguera, A., Fennell, L., Rojas Vera, E. A., & Ramos, V. A. (2016). Progression of the deformation in the southern central Andes (37°S). In A., Folguera M., Naipauer, L. C., Sagripanti, M., Ghiglione, D., Orts, & L., Giambiagi (Eds.), *Growth of the southern Andes* (Vol. 5, pp. 115–132). Springer ESS. https://doi.org/10.1007/978-3-319-23060-3_6

Sagripanti, L., Folguera, A., Giménez, M., Rojas Vera, E. A., Fabiano, J. J., Molnar, N., et al. (2014). Geometry of middle to late Triassic extensional deformation pattern in the Cordillera del Viento (southern central Andes): A combined field and geophysical study. *Journal of Iberian Geology*, *40*(2), 349–366. https://doi.org/10.5209/rev_jige.2014.v40.n2.45305

Sagripanti, L., Rojas Vera, E. A., Gianni, G. M., Folguera, A., Harvey, J. E., Farías, M., & Ramos, V. A. (2015). Neotectonic reactivation of the western section of the Malargüe fold and thrust belt (Tromen volcanic plateau, southern central Andes). *Geomorphology*, *232*, 164–181. https://doi.org/10.1016/j.geomorph.2014.12.022

Sánchez, N., Coutand, I., Turienzo, M., Lebinson, F., Araujo, V., & Dimieri, L. (2017). Retracted: Middle Miocene to early Pliocene contraction in the Chos Malal fold-and-thrust belt (Neuquén basin, Argentina): Insights from structural analysis and apatite fission-tracks thermochronology. *Tectonics*, *36*, 1966–1987. https://doi.org/10.1002/2017TC004516

Sánchez, N., Turienzo, M., Coutand, I., Lebinson, F., Araujo, V., & Dimieri, L. (2020). Structural and thermochronological constraints on the exhumation of the Chos Malal fold and thrust belt (~37° S). In *Opening and closure of the Neuquén Basin in the southern Andes* (pp. 323–340). Springer. https://doi.org/10.1007/978-3-030-29680-3_13

Sánchez, N., Turienzo, M., Lebinson, F., Araujo, V., Coutand, I., & Dimieri, L. (2015). Structural style of the Chos Malal fold and thrust belt, Neuquén basin, Argentina: Relationship between thick- and thin-skinned tectonics. *Journal of South American Earth Sciences*, *64*, 399–417. https://doi.org/10.1016/j.jsames.2015.07.001

Savignano, E., Mazzoli, S., Arce, M., Franchini, M., Gautheron, C., Paolini, M., & Zattin, M. (2016). (Un)Coupled thrust belt-foreland deformation in the northern Patagonian Andes: New insights from the Esquel-Gastre sector (41°30′-43°S). *Tectonics*, *35*, 2636–2656. https://doi.org/10.1002/2016TC004225

Seton, M., Müller, R. D., Zahirovic, S., Gaina, C., Torsvik, T., Shephard, G., et al. (2012). Global continental and ocean basin reconstructions since 200 Ma. *Earth-Science Reviews*, *113*(3–4), 212–270. https://doi.org/10.1016/j.earscirev.2012.03.002

Sigismondi, M. E. (2013). *Estudio de la deformación litosférica de la cuenca Neuquina Estructura termal, datos Hurford dad y sísmica de reflexión*. Facultad de Ciencias Exactas y Naturales Universidad de Buenos Aires. http://digital.bl.fcen.uba.ar/Download/Tesis/Tesis_5361_Sigismondi.pdf

Sigismondi, M., & Ramos, V. A. (2009a). El flujo de calor de la cuenca neuquina, Argentina, segunda parte. *Instituto Argentino del Petróleo y Gas, Petrotecnia*, *2*(9), 58–76.

Sigismondi, M., & Ramos, V. A. (2009b). *El flujo de calor de la cuenca Neuquina, Argentina, primera parte* (Vol. 1, pp. 64–81). Instituto Argentino del Petróleo y Gas.

Silva, A., Ferrari, L., Orozco, T., Bernal, J. P., & Norini, G. (2018). U-Pb, U-Th, and Ar-Ar geochronology of the Domuyo geothermal area, northern Patagonia: Evidence for a voluminous late Pleistocene silicic dome complex. *Poster en South American Symposium on Isotope Geology*.

Silvestro, J., & Zubiri, M. (2008). Convergencia oblicua: Modelo estructural alternativo para la Dorsal Neuquina (39ºS)-Neuquén. *Revista de la Asociación Geológica Argentina*, *63*(1), 49–64.

Somoza, R., & Ghidella, M. E. (2005). Convergencia en el margen occidental de América del sur durante el cenozoico: Subducción de las placas de nazca, farallón y aluk. *Revista de la Asociación Geológica Argentina*, *60*(4), 797–809.

Somoza, R., & Zaffarana, C. B. (2008). Mid-Cretaceous polar standstill of South America, motion of the Atlantic hotspots and the birth of the Andean cordillera. *Earth and Planetary Science Letters*, *271*(1–4), 267–277. https://doi.org/10.1016/j.epsl.2008.04.004

Spagnuolo, M. G., Folguera, A., Litvak, V., Vera, E. A. R., & Ramos, V. A. (2012). Late Cretaceous arc rocks in the Andean retroarc region at 36.5°S: Evidence supporting a late Cretaceous slab shallowing. *Journal of South American Earth Sciences*, *38*, 44–56. https://doi.org/10.1016/j.jsames.2012.05.002

Spikings, R., Dungan, M., Foeken, J., Carter, A., Page, L., & Stuart, F. (2008). Tectonic response of the central Chilean margin (35-38°S) to the collision and subduction of heterogeneous oceanic crust: A thermochronological study. *Journal of the Geological Society*, *165*, 941–953. https://doi.org/10.1144/0016-76492007-115

Steinmann, G. (1929). *Geologie von Peru: Heidelberg* (p. 448). Karl Winter.
Stern, C. R. (2004). Active Andean volcanism: Its geologic and tectonic setting. *Revista Geológica de Chile*, *31*(2), 161–206. https://doi.org/10.4067/s0716-02082004000200001
Strecker, U. (1996). *Studies of Cenozoic continental tectonics: Part I, apatite fission-track thermochronology of the black Hills uplift, south Dakota; Part II. Seismic sequence stratigraphy of the Goshute valley halfgraben, Nevada* (p. 344). University of Wyoming Ph.D. thesis
Tagami, T. (2005). Zircon fission-track thermochronology and applications to fault studies. *Reviews in Mineralogy and Geochemistry*, *58*(1), 95–122. https://doi.org/10.2138/rmg.2005.58.4
Tagami, T., Galbraith, R. F., Yamada, R., & Laslett, G. M. (1998). Revised annealing kinetics of fission tracks in zircon and geological implications. In P. Van den Haute & F. De Corte (Eds.), *Advances in fission-track geochronology* (pp. 99–112). Kluwer Academic Publishers. https://doi.org/10.1007/978-94-015-9133-1_8
Tapia, F., Muñoz, M., Farías, M., Charrier, R., & Astaburuaga, D. (2020). Middle Jurassic-late Cretaceous paleogeography of the western margin of the Neuquén basin (34° 30′-36° S). In *Opening and closure of the Neuquén Basin in the southern Andes* (pp. 269–301). Springer. https://doi.org/10.1007/978-3-030-29680-3_11
Tassara, A., & Yáñez, G. (2003). Relación entre el espesor elástico de la litosfera y la segmentación tectónica del margen andino (15-47°S). *Revista Geológica de Chile*, *30*(2), 159–186. https://doi.org/10.4067/S0716-02082003000200002
ter Voorde, M., de Bruijne, C. H., Cloetingh, S. A. P. L., & Andriessen, P. A. M. (2004). Thermal consequences of thrust faulting: Simultaneous versus successive fault activation and exhumation. *Earth and Planetary Science Letters*, *223*(3–4), 395–413. https://doi.org/10.1016/j.epsl.2004.04.026
Thomson, S. N., Brandon, M. T., Tomkin, J. H., Reiners, P. W., Vásquez, C., & Wilson, N. J. (2010). Glaciation as a destructive and constructive control on mountain building. *Nature*, *467*(7313), 313–317. https://doi.org/10.1038/nature09365
Thomson, S. N., Herve, F., Stockhert, B., Brix, M. R., & Adriasola, A. (2001). *Late Cenozoic tectonic and geomorphic evolution of the Patagonian Andes between 42°S and 52°S, southern Chile assessed using fission-track thermochronology*.
Tunik, M., Folguera, A., Naipauer, M., Pimentel, M., & Ramos, V. A. (2010). Early uplift and orogenic deformation in the Neuquén basin: Constraints on the Andean uplift from U-Pb and Hf isotopic data of detrital zircons. *Tectonophysics*, *489*(1–4), 258–273. https://doi.org/10.1016/j.tecto.2010.04.017
Turienzo, M., Sánchez, N., Lebinson, F., & Dimieri, L. (2018). The structure of the southern central Andes (Chos Malal fold and thrust belt). In *The evolution of the Chilean-Argentinean Andes* (pp. 411–441). Springer. https://doi.org/10.1007/978-3-319-67774-3_17
Utgé, S., Folguera Telichevsky, A., Litvak, V. D., & Ramos, V. A. (2009). Geología del sector norte de la cuenca de cura mallín en las lagunas de epulaufquen Neuquén. *Revista de la Asociacion Geologica Argentina*, *62*(2), 231–248.
Varela, A. N., Raigemborn, M. S., Richiano, S., White, T., Poiré, D. G., & Lizzoli, S. (2018). Late Cretaceous paleosols as paleoclimate proxies of high-latitude southern hemisphere: Mata amarilla formation, Patagonia, Argentina. *Sedimentary Geology*, *363*, 83–95. https://doi.org/10.1016/j.sedgeo.2017.11.001
Vergani, G. D., Tankard, A. J., Belotti, H. J., & Welsink, H. J. (1995). *Tectonic evolution and paleogeography of the Neuquén Basin, Argentina* (pp. 383–402). https://doi.org/10.1306/M62593C19
Vergara, M., Levi, B., Nyström, J. O., & Cancino, A. (1995). Jurassic and early Cretaceous island arc volcanism, extension, and subsidence in the coast range of central chile. *Geological Society of America Bulletin*, *107*(12), 1427–1440. https://doi.org/10.1130/0016-7606(1995)107<1427:jaecia>2.3.co;2
Vermeesch, P. (2018). IsoplotR: A free and open toolbox for geochronology. *Geoscience Frontiers*, *9*, 1479–1493. https://doi.org/10.1016/j.gsf.2018.04.001
Wolf, R. A., Farley, K. A., & Kass, D. M. (1998). Modeling of the temperature sensitivity of the apatite (U-Th)/He thermochronometer. *Chemical Geology*, *148*, 105–114. https://doi.org/10.1016/s0009-2541(98)00024-2
Zamora Valcarce, G. (2007). *Estructura y Cinemática de la faja plegada y corrida del Agrio, Cuenca Neuquina* (PhD thesis,p. 303). Universidad de Buenos Aires.
Zamora Valcarce, G., Zapata, T., del Pino, D., & Ansa, A. (2006). Structural evolution and magmatic characteristics of the Agrio fold and thrust belt. In S. M. Kay & V. A. Ramos (Eds.), *Evolution of an Andean margin: A tectonic and magmatic view from the Andes to the Neuquén Basin (35°-39°S)* (Vol. 407, pp. 125–145). Geological Society of America, Special Paper. https://doi.org/10.1130/2006.2407(06)
Zamora Valcarce, G., Zapata, T., Ramos, V. A., Rodríguez, F., & Bernardo, M. L. (2009). Evolución tectónica del frente andino en Neuquén. *Revista de Asociación Geológica Argentina*, *65*, 192–203.
Zapata, T., Brissón, I., & Dzelalija, F. (1999). The role of basement in the Andean fold and thrust belt of the Neuquén basin. *Thrust Tectonics*, *99*, 122–124.
Zappettini, E., Méndez, V., & Zanettini, J. C. (1987). Metasedimentitas mesopaleozoicas en el noroeste de la provincia del neuquén. *Revista de la Asociación Geológica Argentina*, *42*(1–2), 206–207.
Zappettini, E. O., Chernicoff, C. J., Santos, J. O. S., Dalponte, M., Belousova, E., & McNaughton, N. (2012). Retrowedge-related carboniferous units and coeval magmatism in the northwestern Neuquén province, Argentina. *International Journal of Earth Sciences (Geol Rundsch)*, *101*(8), 2083–2104. https://doi.org/10.1007/s00531-012-0774-3

References from the Supporting Information

Barbarand, J., Hurford, A. J., & Carter, A. (2003). Variation in apatite fission-track length measurement: Implications for thermal history modelling. *Chemical Geology*, *198*, 77–106.
Dahl, P. S. (1997). A crystal-chemical basis for Pb retention and fission-track annealing systematics in U-bearing minerals, with implications for geochronology. *Earth and Planetary Science Letters*, *150*(3–4), 277–290.
De Grave, J. (2003). *Apatite fission-track thermochronology of the Altai mountains (south Siberia, Russia) and the Tien Shan mountains (Kyrgyzstan): Relevance to Meso-Cenozoic tectonics and denudation in central Asia (Doctoral dissertation)*. Ghent University.
Dobson, K. J., Stuart, F. M., & Dempster, T. J. (2008). U and Th zonation in Fish Canyon Tuff zircons: Implications for a zircon (U–Th)/He standard. *Geochimica et Cosmochimica Acta*, *72*(19), 4745–4755.
Gleadow, A. J. (1981). Fission-track dating methods: What are the real alternatives? *Nuclear Tracks*, *5*(1–2), 3–14.
Hourigan, J. K., Reiners, P. W., & Brandon, M. T. (2005). U-Th zonation-dependent alpha-ejection in (U-Th)/He chronometry. *Geochimica et Cosmochimica Acta*, *69*(13), 3349–3365.
Pupin, J. P. (1980). Zircon and granite petrology. *Contributions to Mineralogy and Petrology*, *73*(3), 207–220.

Sláma, J., Košler, J., Condon, D. J., Crowley, J. L., Gerdes, A., Hanchar, J. M., et al. (2008). Plesovice zircon—A new natural reference material for U-Pb and Hf isotopic microanalysis. *Chem Geology*, *249*(7), 1–35.

Tagami, T., Lal, N., Sorkhabi, R. B., Ito, H., & Nishimura, S. (1988). Fission track dating using external detector method: A laboratory procedure. *Memoirs of the Faculty of Science, Kyoto University*, *53*, 14–30.

Wiedenbeck, M., Hanchar, J. M., Peck, W. H., Sylvester, P., Valley, J., Whitehouse, M., et al. (2004). Further characterisation of the 91500 zircon crystal. *Geostandards and Geoanalytical Research*, *28*(1), 9–39.

Zhou, R., Schoenbohm, L. M., Sobel, E. R., Davis, D. W., & Glodny, J. (2017). New constraints on orogenic models of the southern Central Andean Plateau: Cenozoic basin evolution and bedrock exhumation. *Geological Society of America Bulletin*, *129*, 152–170. https://doi.org/10.1130/B31384.1